A Search for Supersymmetry in CMS Photon +Jet + ME_T Events

Rachel Yohay
University of Virginia
March 29, 2012

Outline

- Detecting photons with the CMS ECAL
  - Distinct challenges of the ECAL endcaps
- SUSY photon + jet + ME_T search
  - Motivation
  - Event selection
  - Background estimation
  - Results
  - Interpretation

ECAL operating principles

[1]

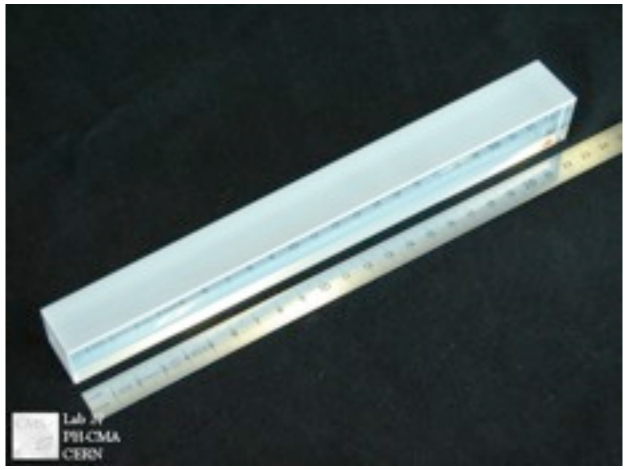

$PbWO_4$ crystal

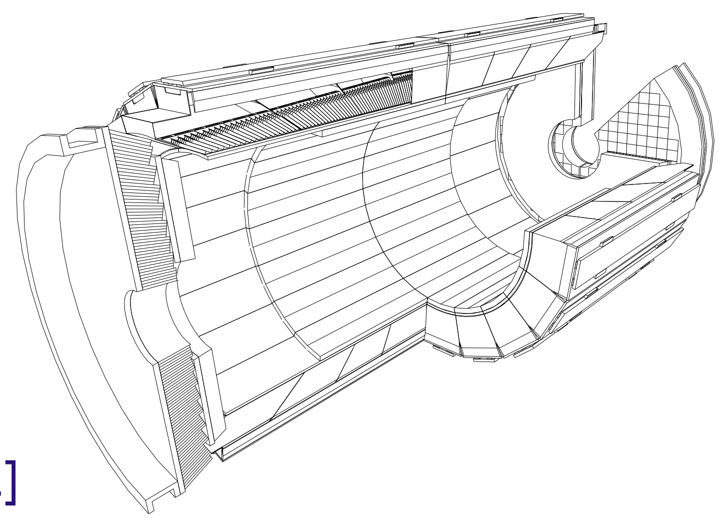

[2]

Fig. 1.5: A 3-D view of the electromagnetic calorimeter.

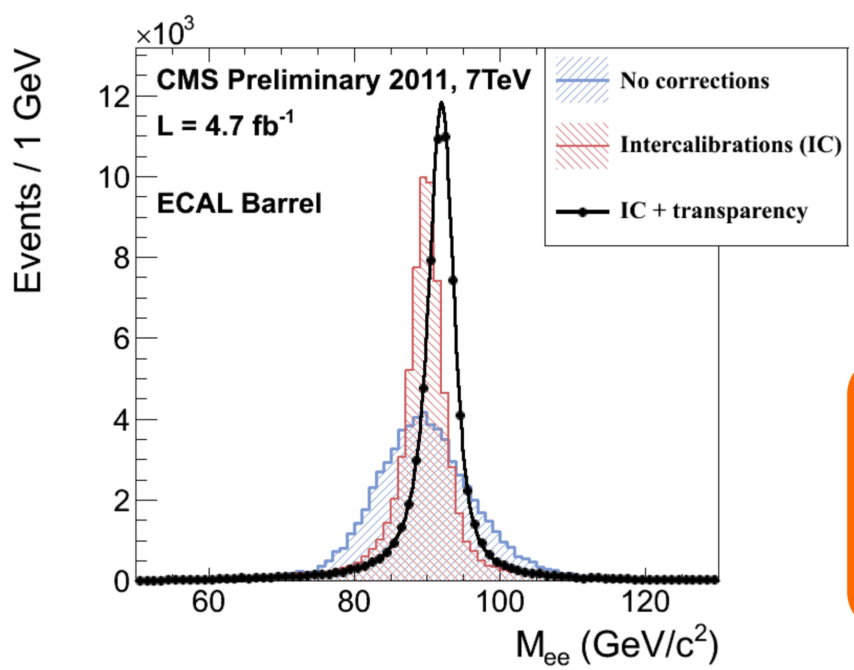

[3]

- Constructed of ~75,000 compact, dense (8.3 g/cm^3), relatively radiation hard scintillating lead tungstate ($PbWO_4$) crystals
- Crystal dimensions: ~1 Molière radius (~22 mm) x ~1 Molière radius x ~25 X_0 (~9 mm) ⇒ most of an

  electromagnetic shower is contained within 1 crystal
- Short scintillation time (~80% of scintillation light is emitted in 25 ns, the LHC collision frequency) ⇒ can

  easily resolve events in different LHC buckets

Energy resolution: Goal: **0.05**

$(\sigma/E)^2 = (a/\sqrt{E})^2 + (b/E)^2 + c^2$

Distinct challenges of the ECAL endcaps

[4]

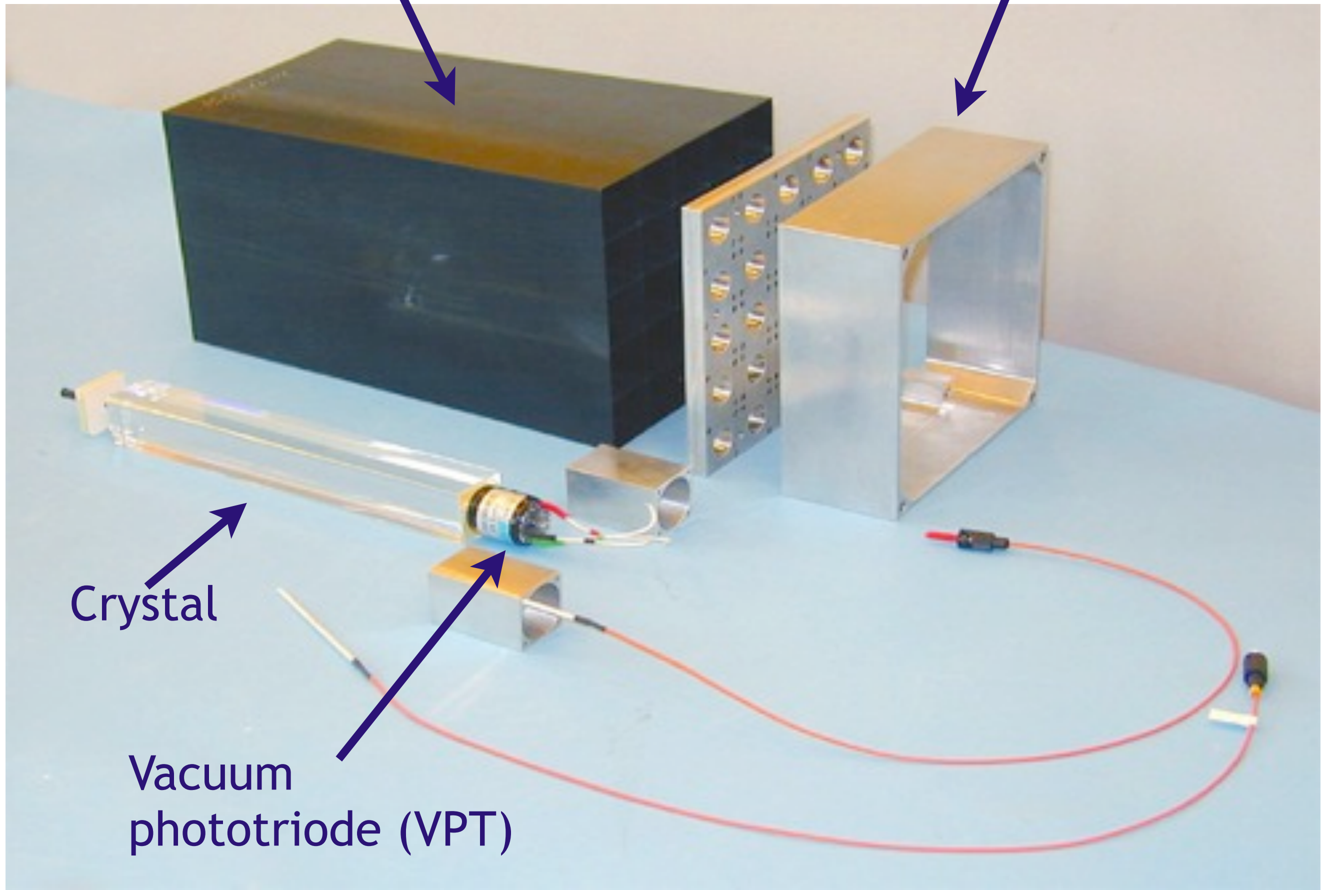

Disassembled EE supercrystal

- ECAL endcaps extend crystal coverage from η = 1.5 out to η = 3.0
  - Larger acceptance for rare $H\rightarrow\gamma\gamma$, $H\rightarrow ZZ$, and $H\rightarrow WW$ processes
  - Calorimetry at high η (+ particle flow techniques) $\Rightarrow$ better ME_T reconstruction

    $\Rightarrow$ better sensitivity to SUSY processes
- EE faces a much harsher environment than EB
  - Strong magnetic field
  - Higher occupancy
  - More radiation damage
- **Significant design difference between EB and EE: choice of vacuum phototriode as photodetector**
- Calibrating EE is a considerable challenge

Anode, dynode, and cathode HV wires

[5]

Faceplate

[6]

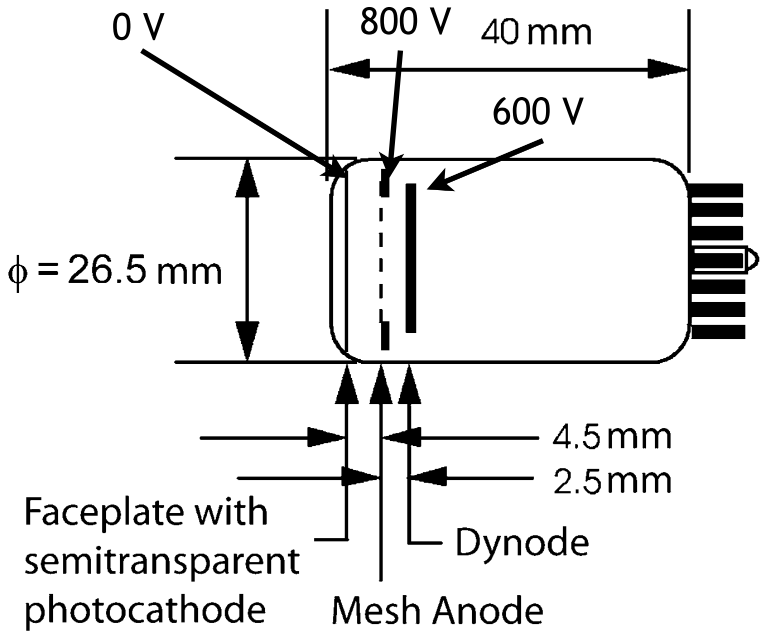

Schematic of a CMS VPT

- Chosen for their radiation hardness and good performance in strong magnetic fields
- Cathode at 0 V, dynode at 600 V, and anode mesh between them at 800 V

VPT testing at UVa

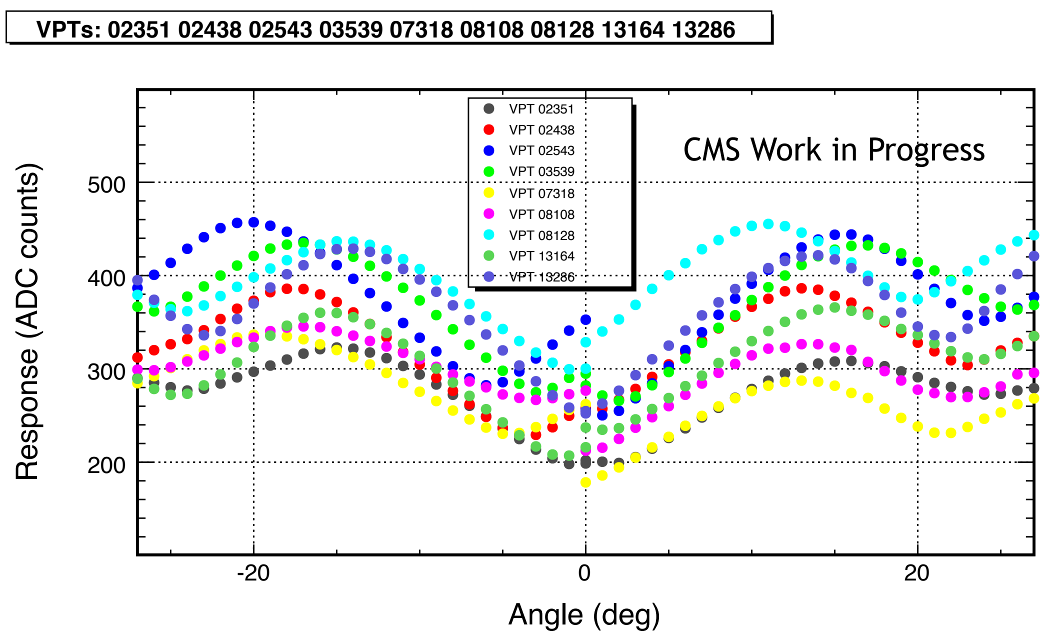

Response of 9 VPTs vs. angle of VPT with respect to the magnetic field direction

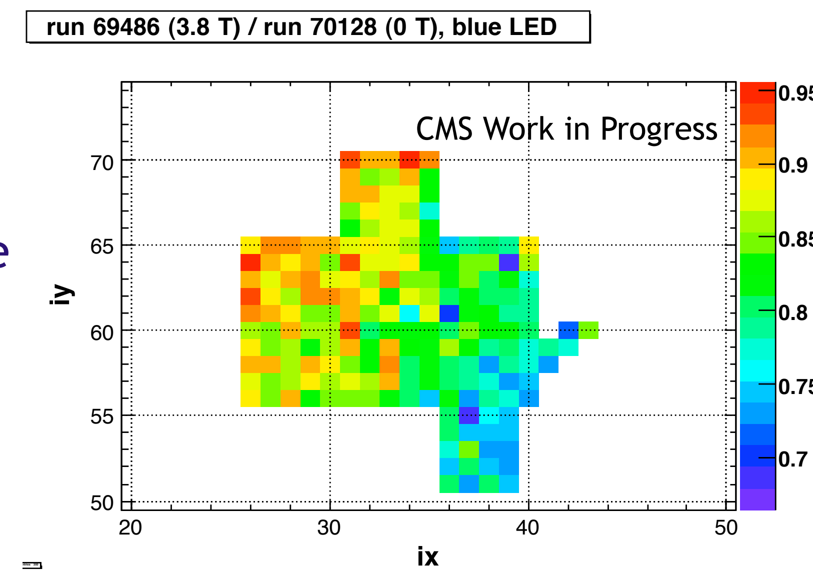

B field effect in one section of EE

- During the spring of 2008, extensive VPT testing was carried out in the UVa 4 T magnet, commissioned during winter 2008-2009
- Certified VPTs were installed on the endcap crystals
- Issues to be understood:
  - Response vs. angle with respect to the magnetic field direction: is it smooth and in rough agreement with theoretical calculation?
  - How do VPTs with skewed anodes or crinkled anodes compare to nominal?

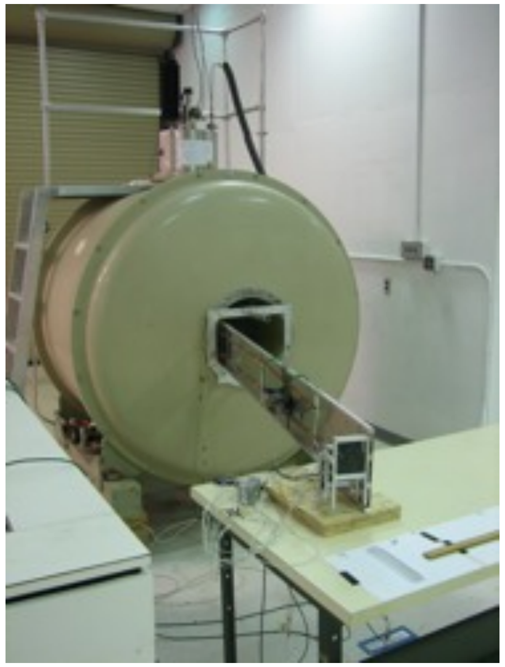

[7]

Apparatus for measuring VPT response vs. angle

VPT stability

- VPTs first used in the OPAL electromagnetic calorimeter endcaps [8]
- VPT gain varies with frequency/amplitude of incident light [9]
  - Effect strongly suppressed in 4 T magnetic field
  - High→low frequency: gain increases
  - Low→high frequency: gain increases or decreases
- All VPT responses are different
- **Provide a constant rate of stability LED pulses to the VPTs to suppress gain changes at LHC on/off transitions**

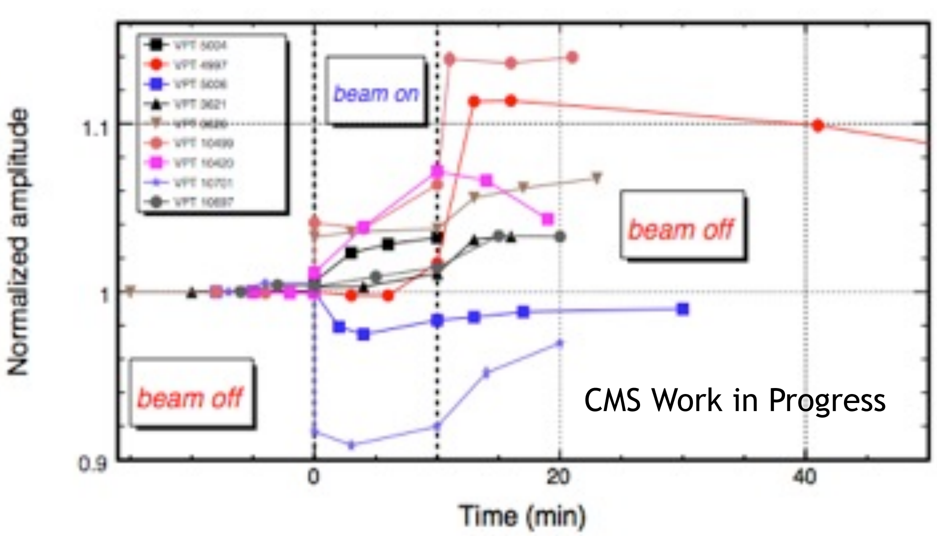

VPT response vs. time for different background pulsing rates

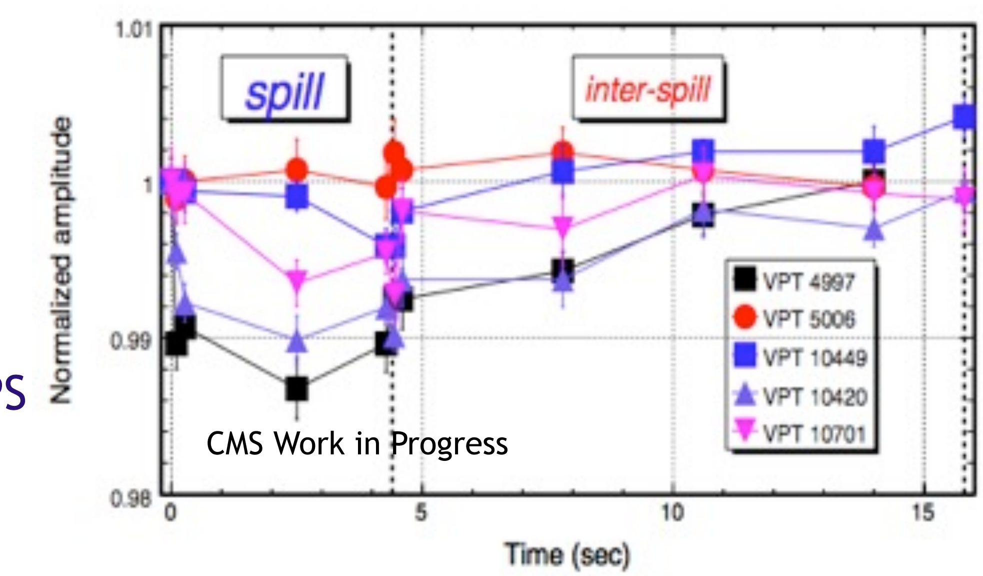

Response of VPTs to SPS spill simulation

Radiation damage

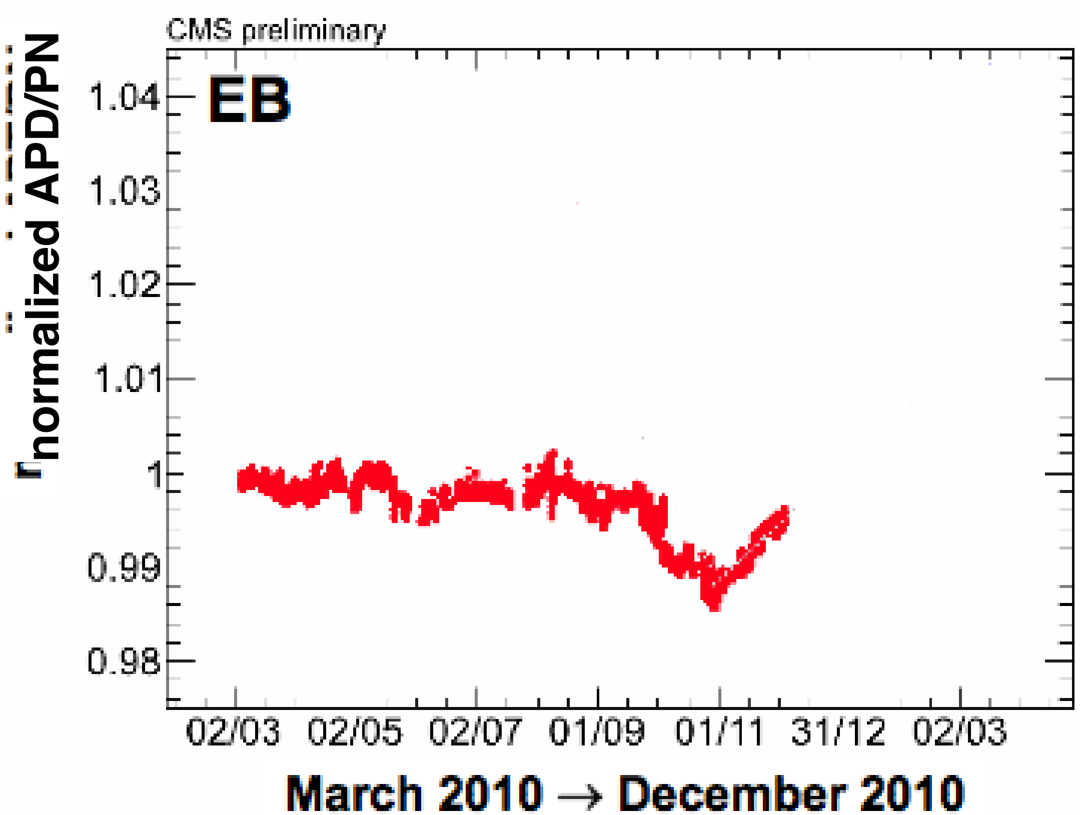

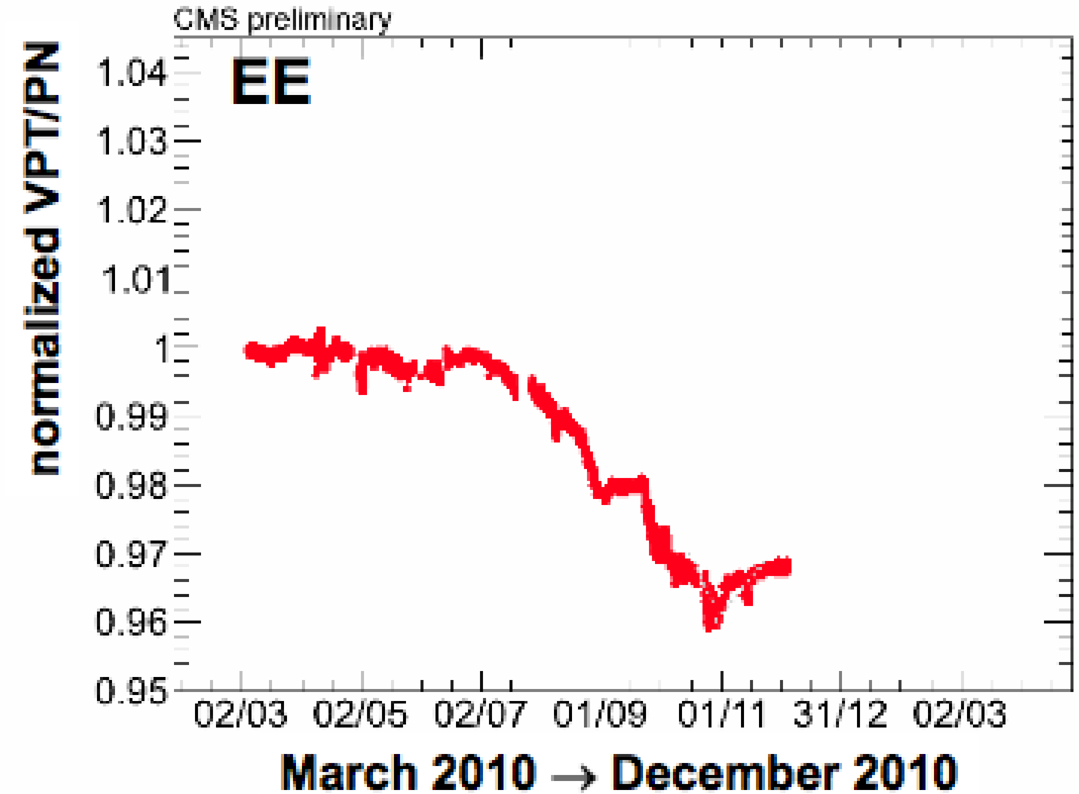

[10]

- Sustained ionizing radiation causes crystal radiation damage, reducing crystal transparency and ultimately the amount of light collected by the photodetectors
- Crystal transparency loss correlated with LHC integrated luminosity, and increases faster for higher instantaneous luminosity
- Continuously pulse crystals from known light source to track and correct for transparency loss from radiation damage

LED stability and calibration system

- Dual wavelength LED stability and monitoring system designed at UVa
    - Blue (450 nm) LED: near the peak of crystal scintillation and VPT photocathode efficiency, so ideal for transmitting the maximum amount of light to VPTs for stability pulsing
    - Orange (617 nm): transparent to crystals but still efficient for VPT photocathode, so ideal for disentangling crystal damage from VPT gain changes
- PN diodes for normalization

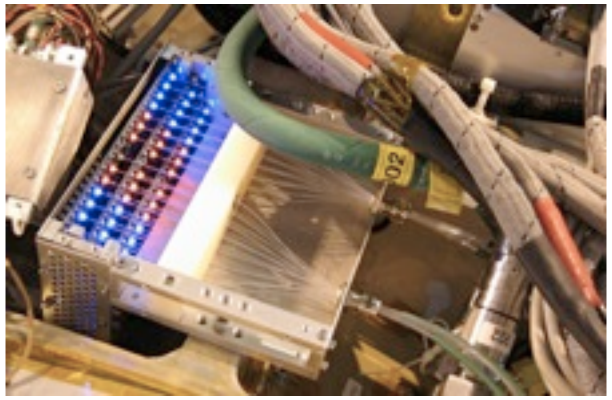

LED system on EE dee patch panel

[12]

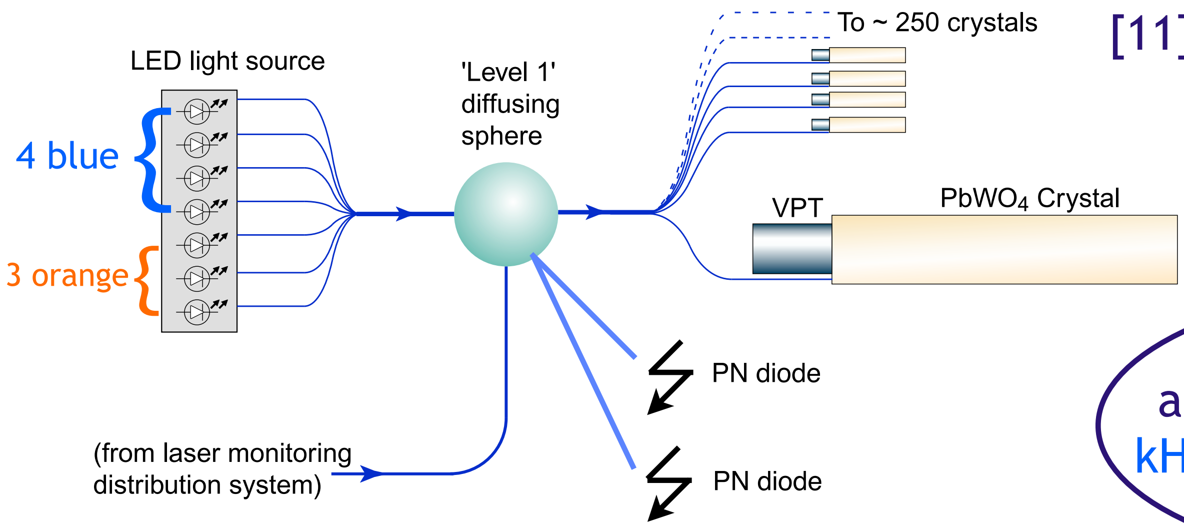

[11]

summary

	LED	Beam LOW	Beam HIGH
Red:	88.4 Hz	200-300 Hz	16-18 kHz
Green:	635 Hz	190-220 Hz	8.0-8.5 kHz
Blue:	932 Hz	220-260 Hz	15-16 kHz

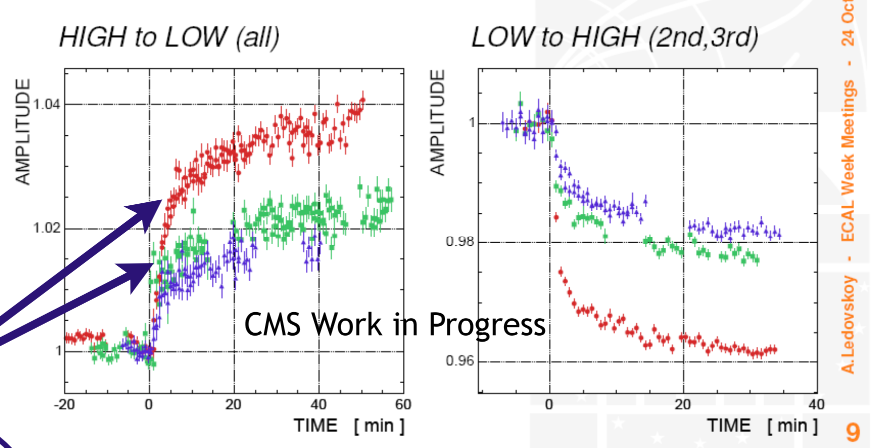

classic VPT effect approximately halved for ~1 kHz stability pulse vs. ~100 Hz stability pulse

Hardware setup

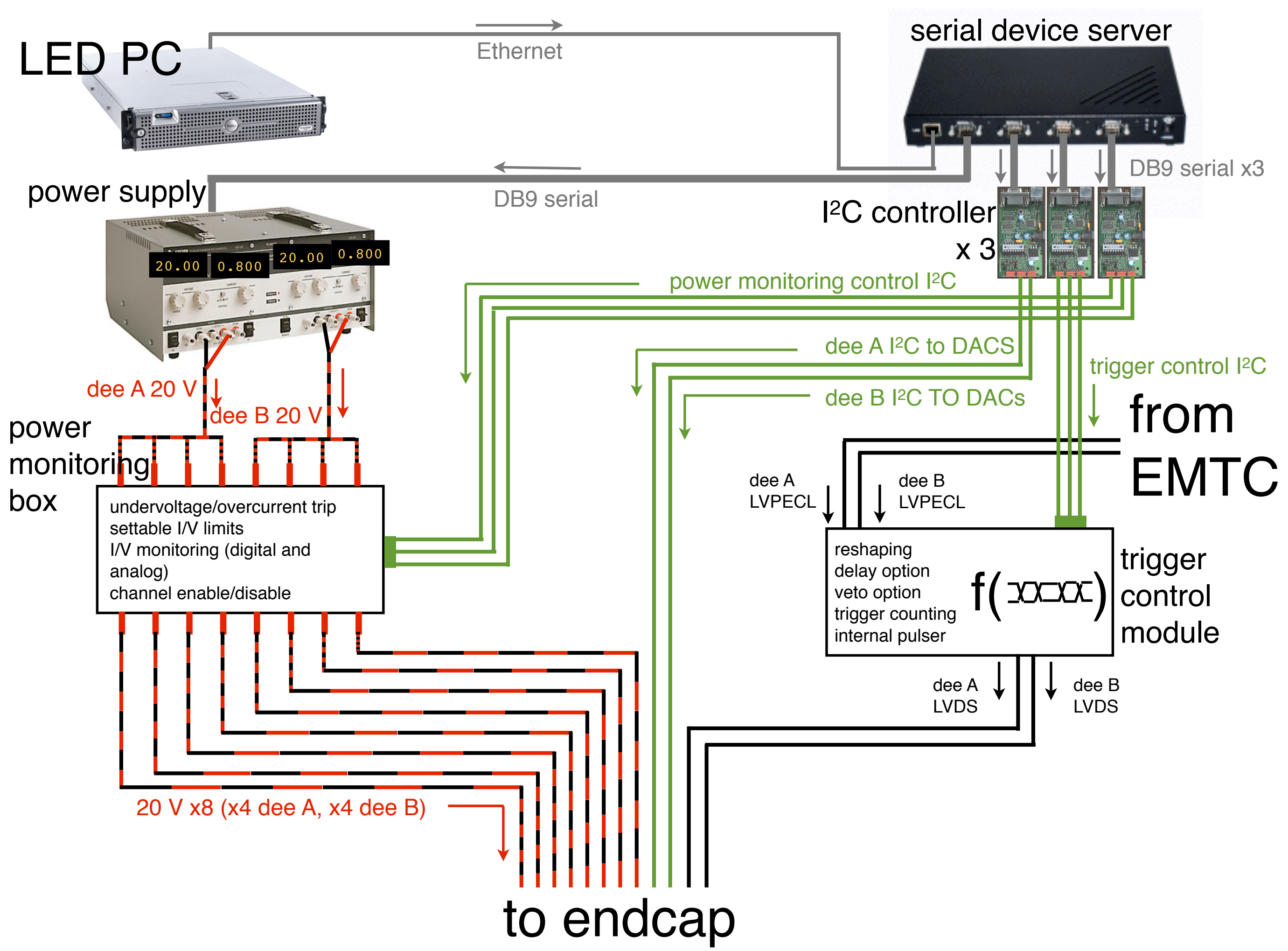

- LED amplitudes set via I^{2}C commands communicated to the hardware via Ethernet-to-serial and serial-to-I^{2}C bridges
- Trigger pulse originates in counting room and is regenerated on the LED circuit board on the detector

Control and monitoring software

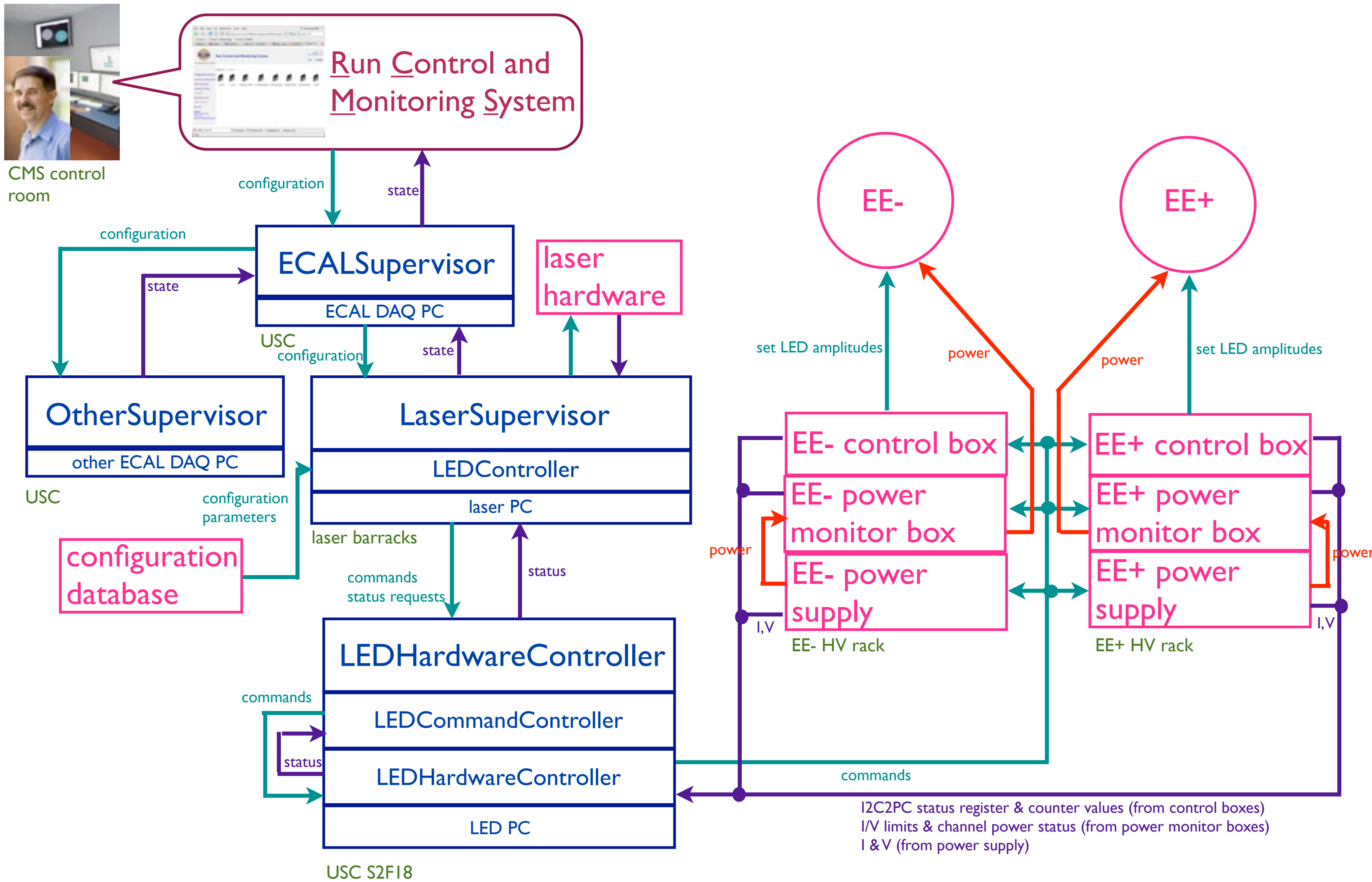

- Use existing LaserSupervisor XDAQ executive as interface to ECAL DAQ
- Execute LED on/off commands sent from the LaserSupervisor
- Monitoring of electronics every 10 minutes

Control and monitoring software

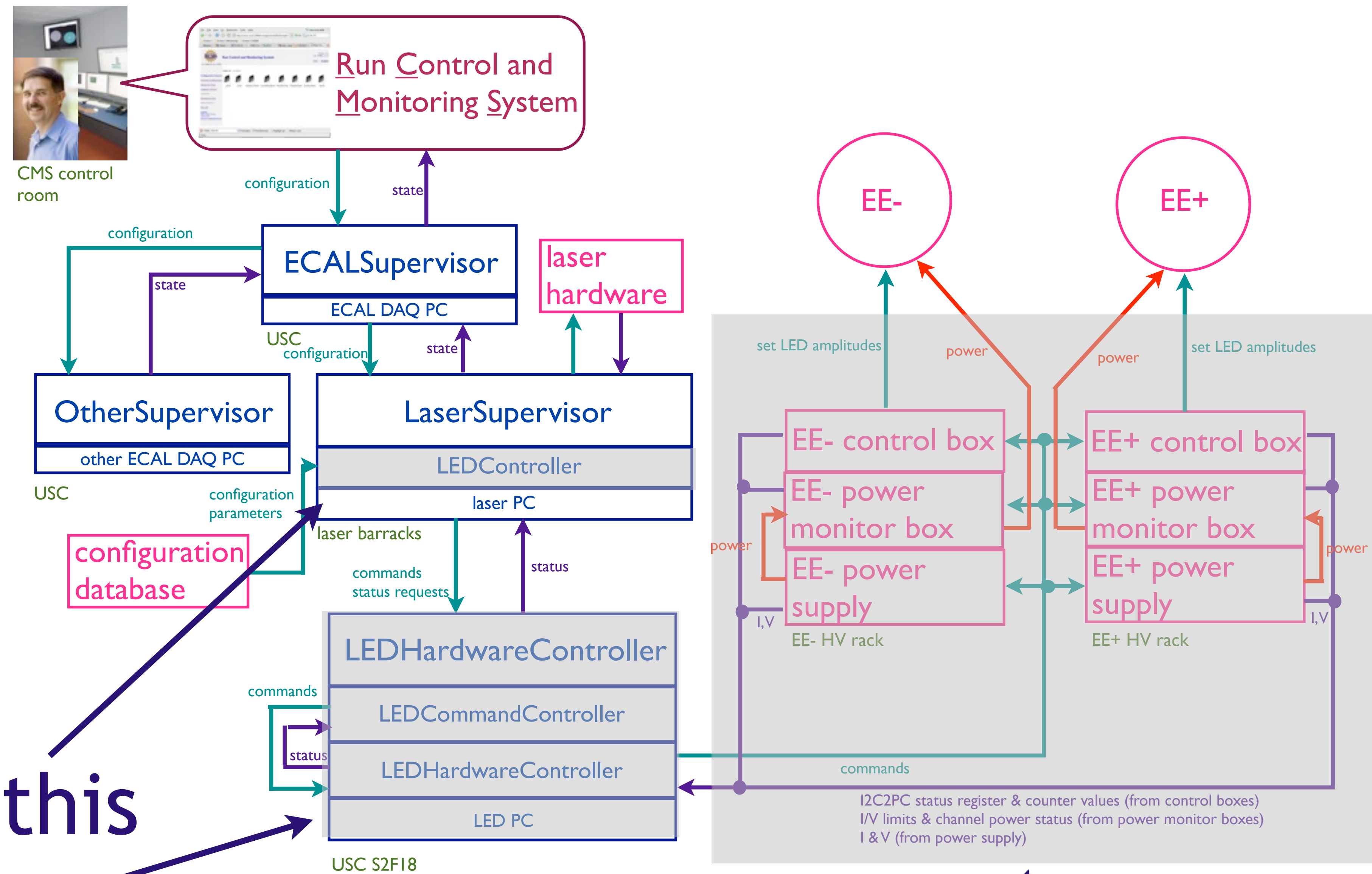

Wrote this software

Wrote monitoring programs to assess the health of this hardware

LED and VPT performance

VPT/PN vs. time for blue laser (green) and blue LED (blue) Apr. 17 - May 2 2011

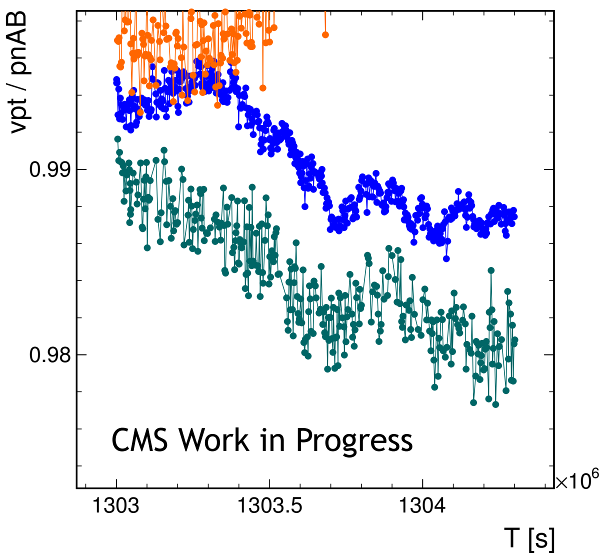

Ratio of PN-normalized VPT amplitudes for two different runs (channels experienced HV and B field cycling between runs)

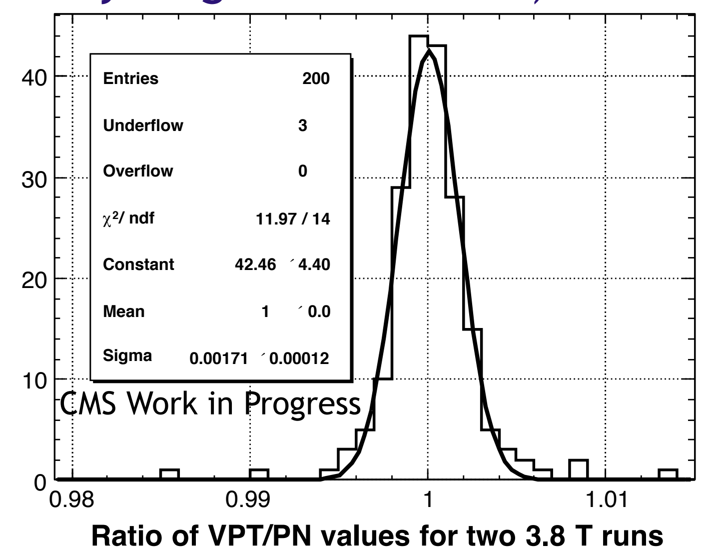

Distribution of average LED timing for a single diffusing sphere

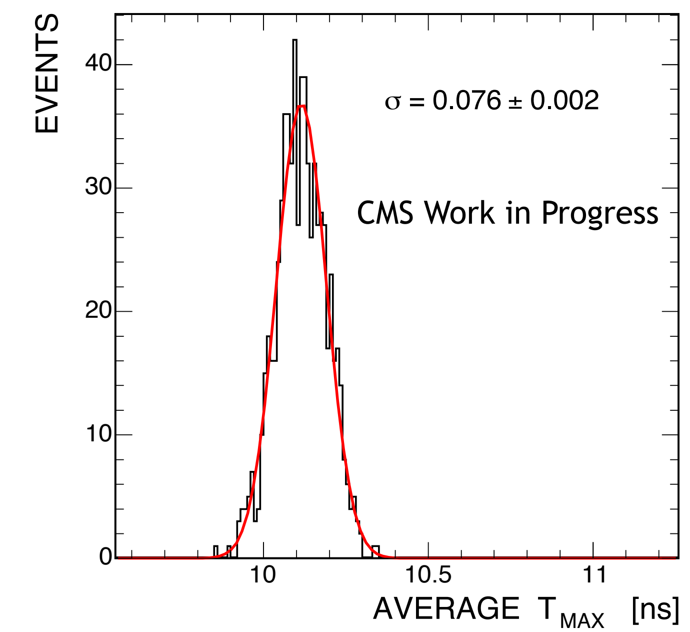

- Stable, reliable LED system important for ECAL calibration
- VPT effect currently dwarfed by transparency loss, but system in place to mitigate gain changes in order to achieve best performance

SUSY with photons

- Why search for supersymmetry?
  - Provides a way to control loop corrections to the Higgs mass
  - Provides a stable, feebly interacting particle ⇒ dark matter candidate
- SUSY particles are heavier than their SM counterparts, so SUSY is a broken symmetry
  - In gauge-mediated SUSY breaking (GMSB), ordinary gauge interactions link the SUSY-breaking and visible sectors
  - **~eV-keV gravitino is the lightest SUSY particle ⇒ escapes CMS undetected, leading to large ME_T**
  - **Neutralino is the next-to-lightest SUSY particle (NLSP) ⇒ neutralino usually decays to photon + gravitino**

[13]

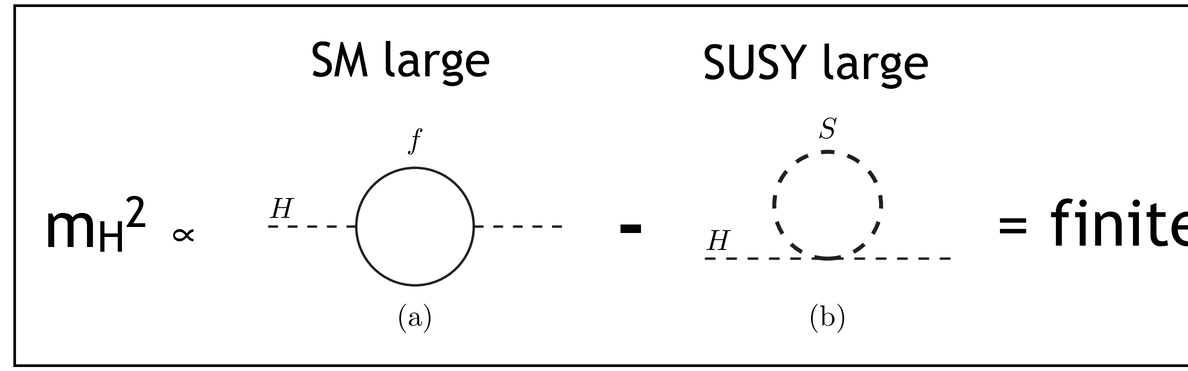

Example of Higgs mass regularization via a SUSY loop that cancels its SM counterpart loop.

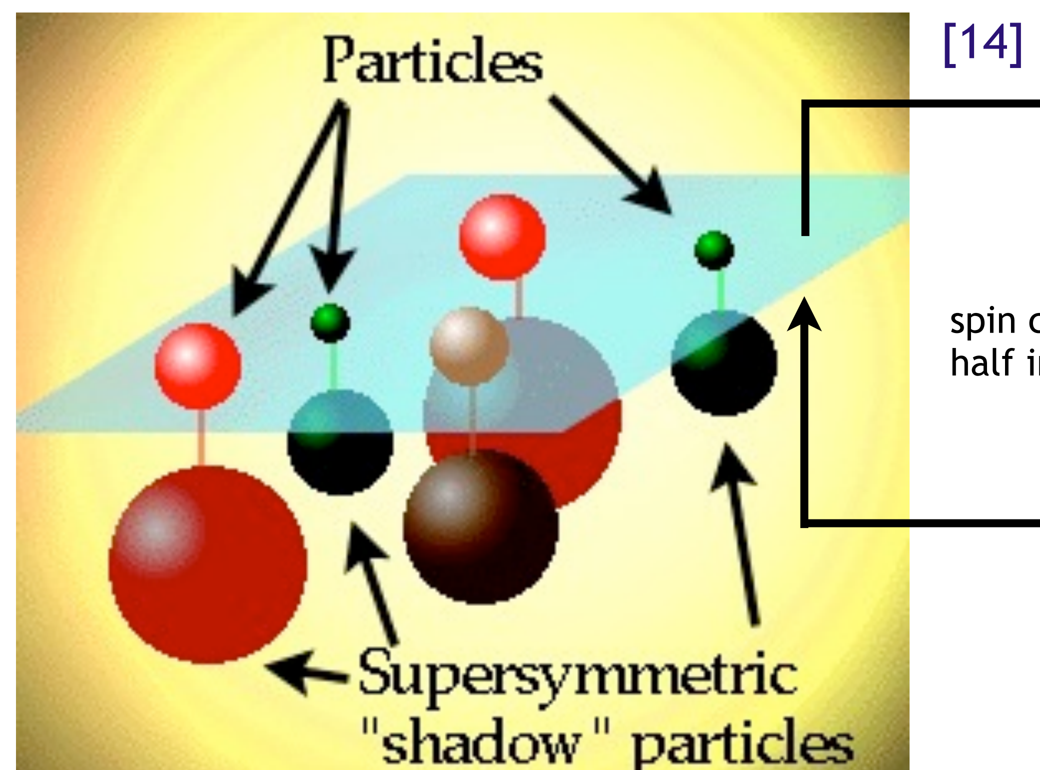

[14]

GMSB final states

2γ+jets+ME_T

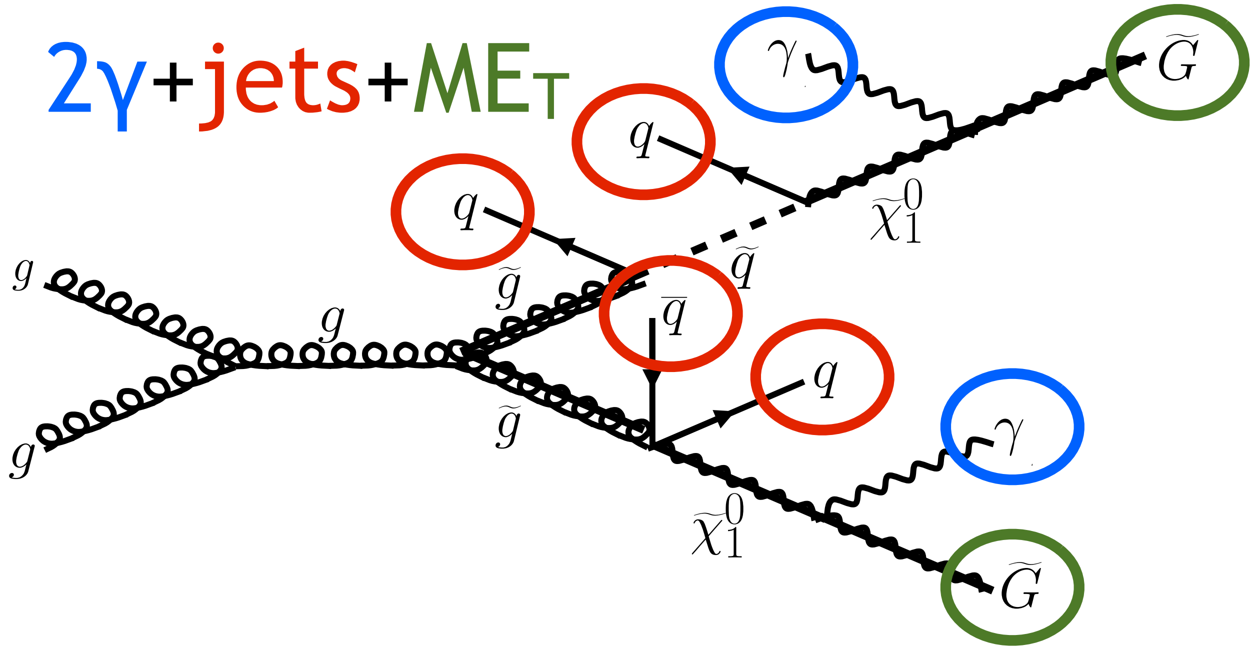

Bino NLSP: neutralino→**γ+gravitino**

l+γ+jets+ME_T

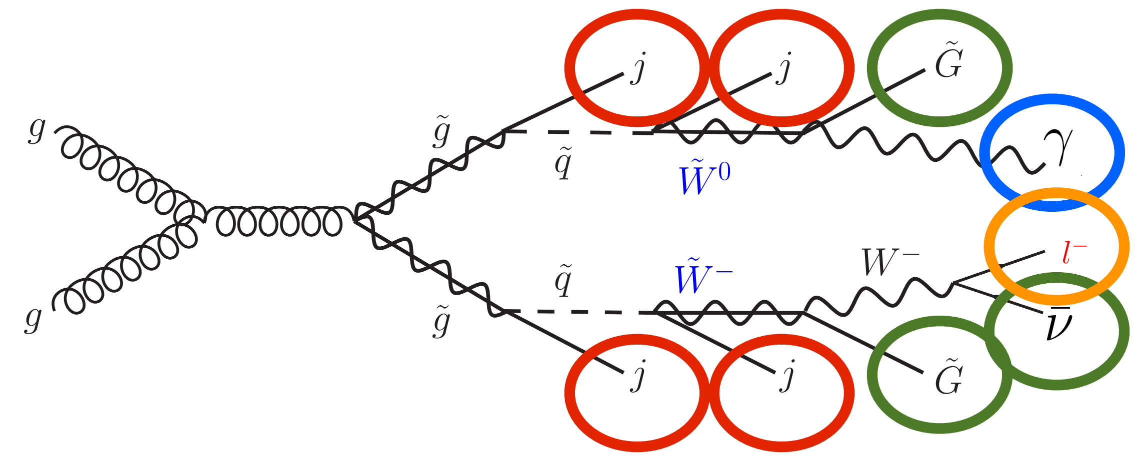

Wino NLSP: neutralino→**γ+gravitino and**
chargino→**W(→lν)+gravitino**

γ+jets+ME_T

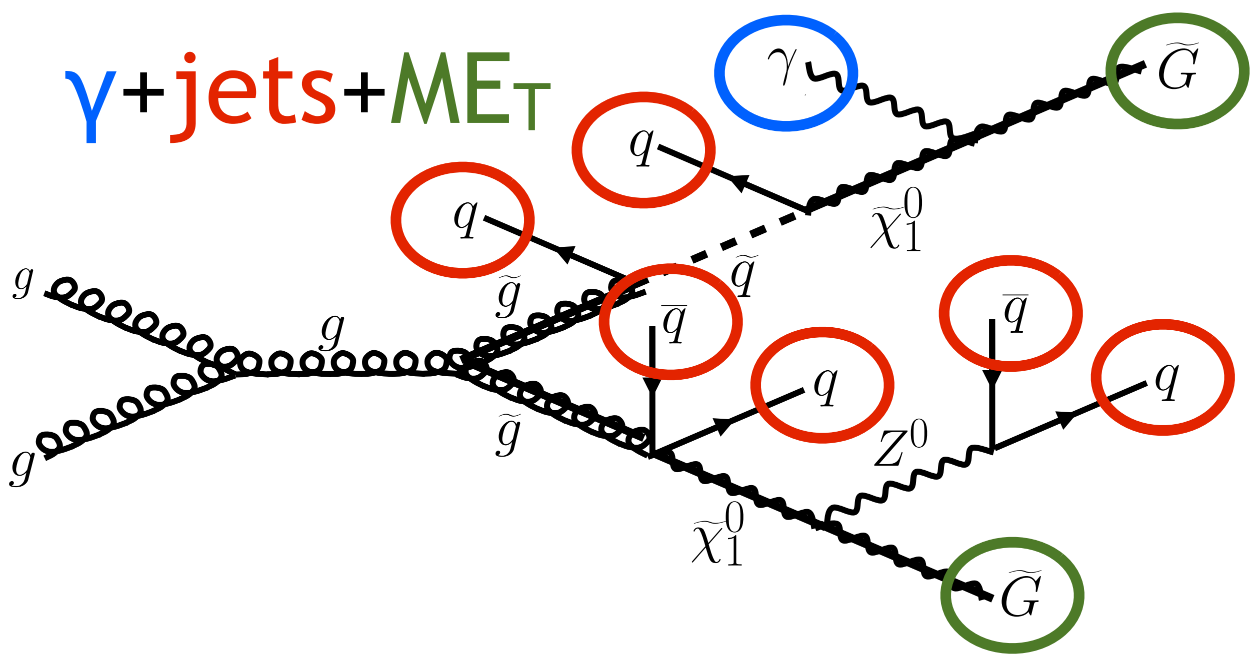

Bino NLSP: neutralino→**γ+gravitino or**
neutralino→**Z(→jets)+gravitino**

γ+jets+ME_T

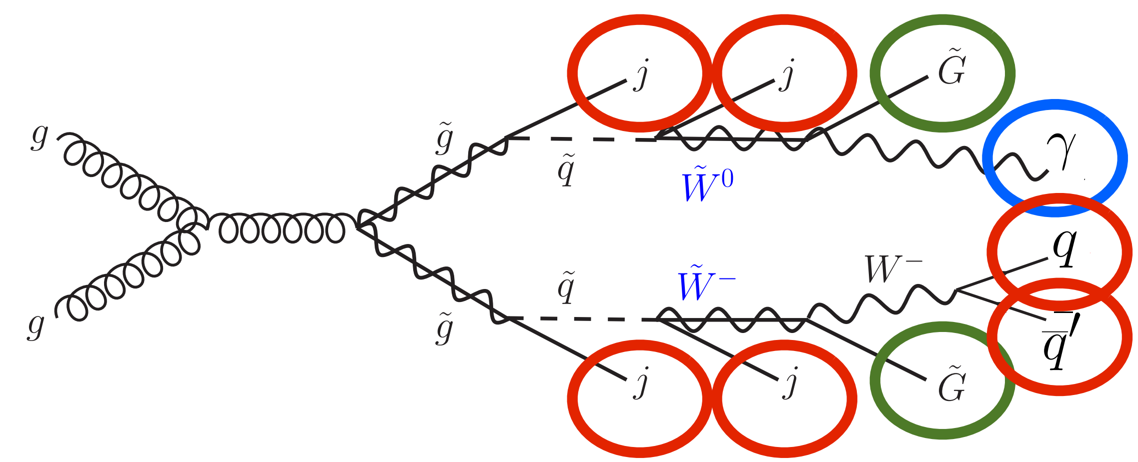

Wino NLSP: neutralino→**γ+gravitino and**
chargino→**W(→jets)+gravitino**

GMSB final states

2γ+jets+ME$_T$

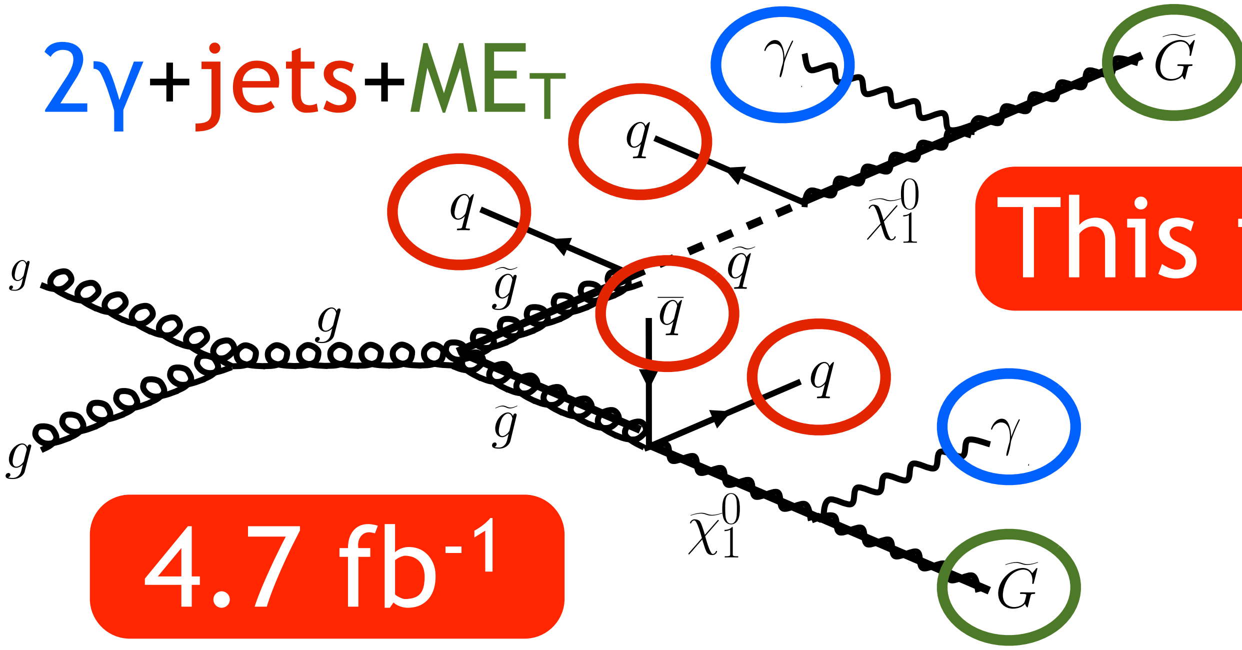

This talk

4.7 fb^{-1}

Bino NLSP: neutralino→**γ+gravitino**

l+γ+jets+ME$_T$

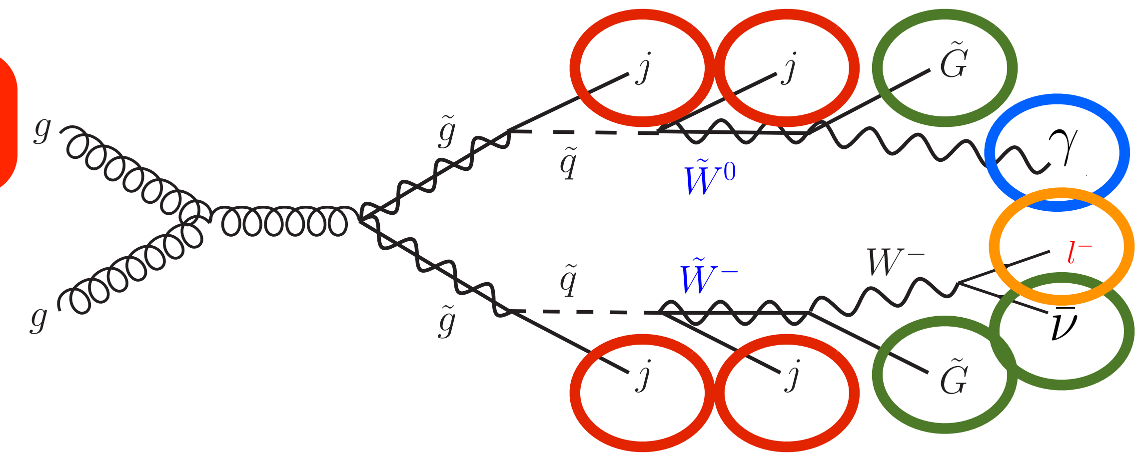

Wino NLSP: neutralino→**γ+gravitino and**
chargino→**W(→lν)+gravitino**

γ+jets+ME$_T$

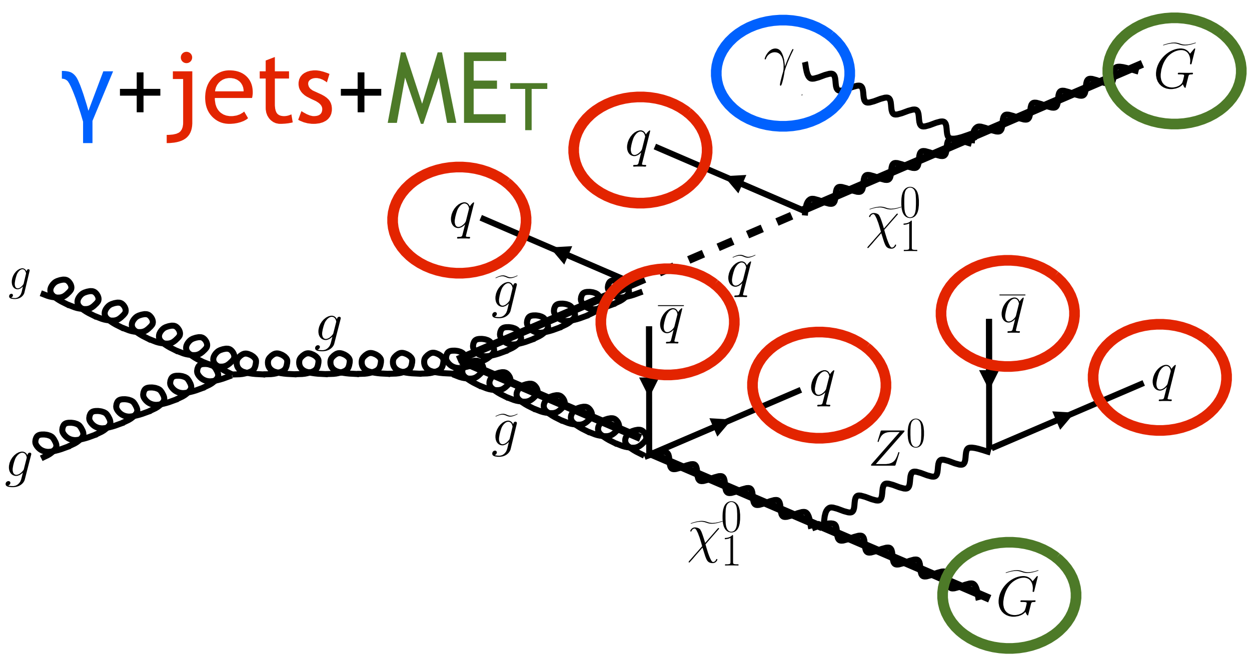

Bino NLSP: neutralino→**γ+gravitino or**
neutralino→**Z(→jets)+gravitino**

γ+jets+ME$_T$

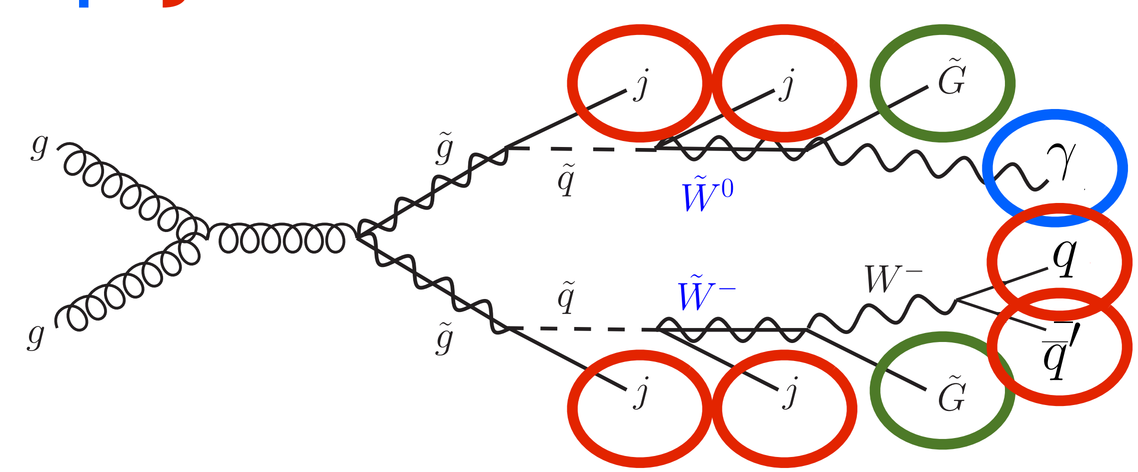

Wino NLSP: neutralino→**γ+gravitino and**
chargino→**W(→jets)+gravitino**

Photon selection

- Single L1-seeded diphoton triggers with 36 and 22 GeV thresholds
- Combined detector isolation cuts in ΔR = 0.3 cone to improve acceptance in jet-rich events
- Shower shape cuts further reduce jet fakes and anomalous energy deposits
- Pileup subtraction from isolation cone using Fastjet [15]
- Minimum ΔR between the photons to avoid isolation cone overlap
- ~±3 ns timing cut removes cosmics and beam halo
- Pixel veto rejects electrons

HLT match	IsoVL
E_T	$> 40/$ > 25 GeV
SC $\|\eta\|$	< 1.4442
H/E	< 0.05
$R9$	< 1
Pixel seed	No/No
I_{comb}, $\sigma_{i\eta i\eta}$	< 6 GeV && < 0.011
JSON	Yes
No. good PVs	≥ 1
ΔR_{EM}	> 0.6
$\Delta\phi_{\mathrm{EM}}$	≥ 0.05

Photon ID efficiency

- Photon ID efficiencies taken from MC and corrected by (data electron efficiency)/(MC electron efficiency)
  - Use $Z \rightarrow ee$ events to measure the electron efficiencies
  - Photon ID cuts designed to behave similarly for electrons and photons
- Signal MC acceptance × efficiency multiplied by 1 factor of $\varepsilon_{data}/\varepsilon_{MC}$ per photon
- Pixel match veto efficiency estimated from MC: $(96.4 \pm 0.5)\%$ (stat. $\oplus$ syst. due to tracker material budget variation)
- Data/MC efficiency scale factor: **0.99 ± 0.04**, with errors due to:
  - Z signal and background shape variation
  - Signal fit over/underestimation
  - Pileup effects
  - MC electron/photon difference

Photon ID scale factor dependence

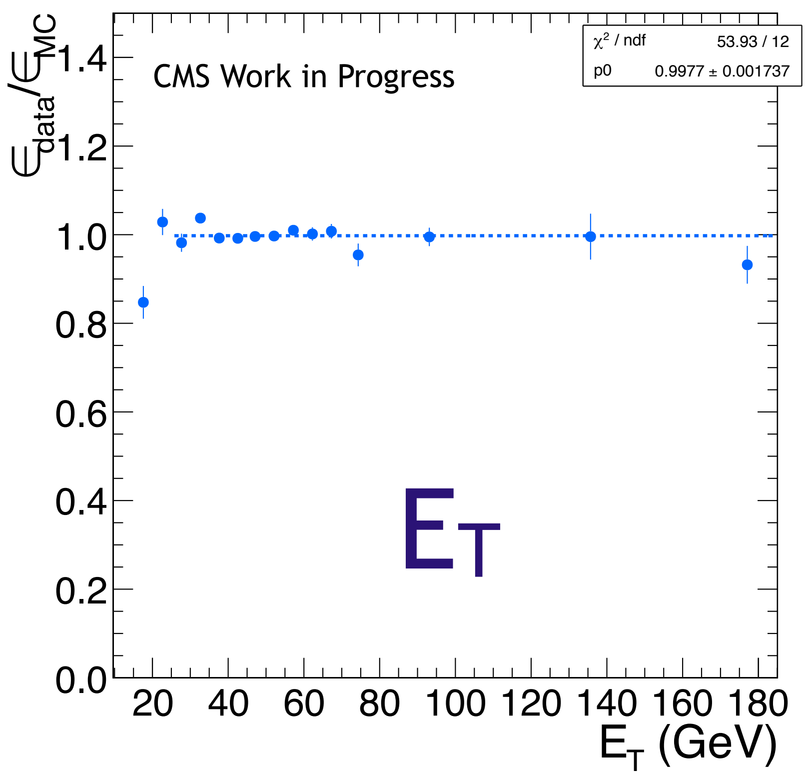

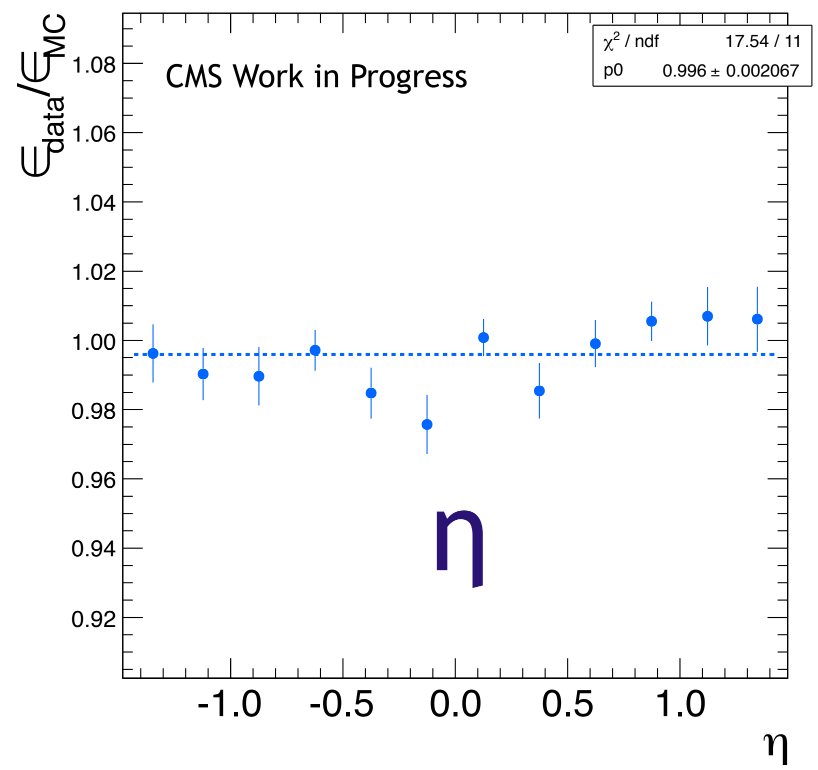

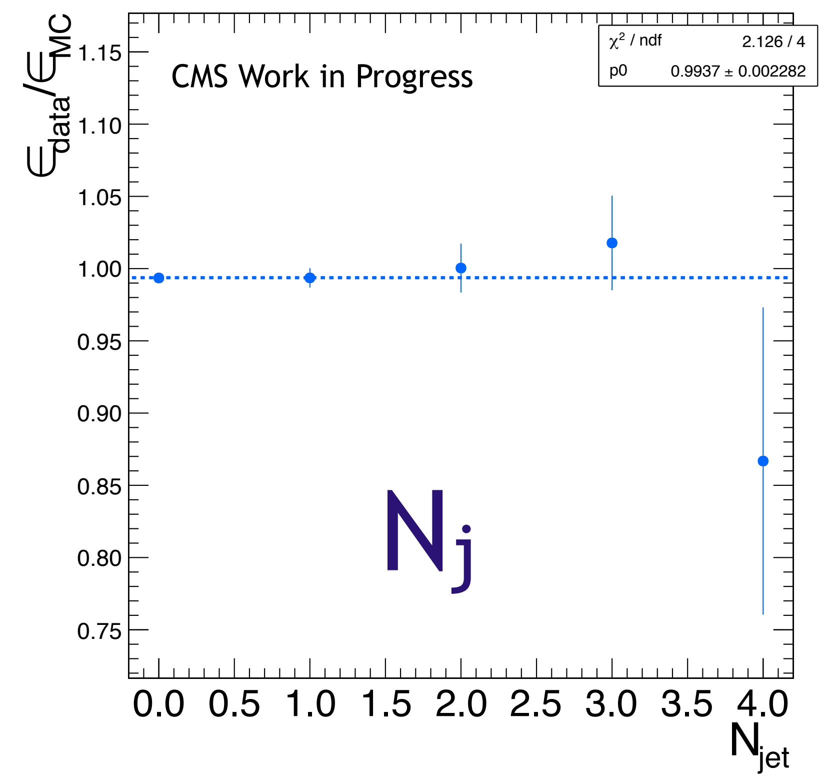

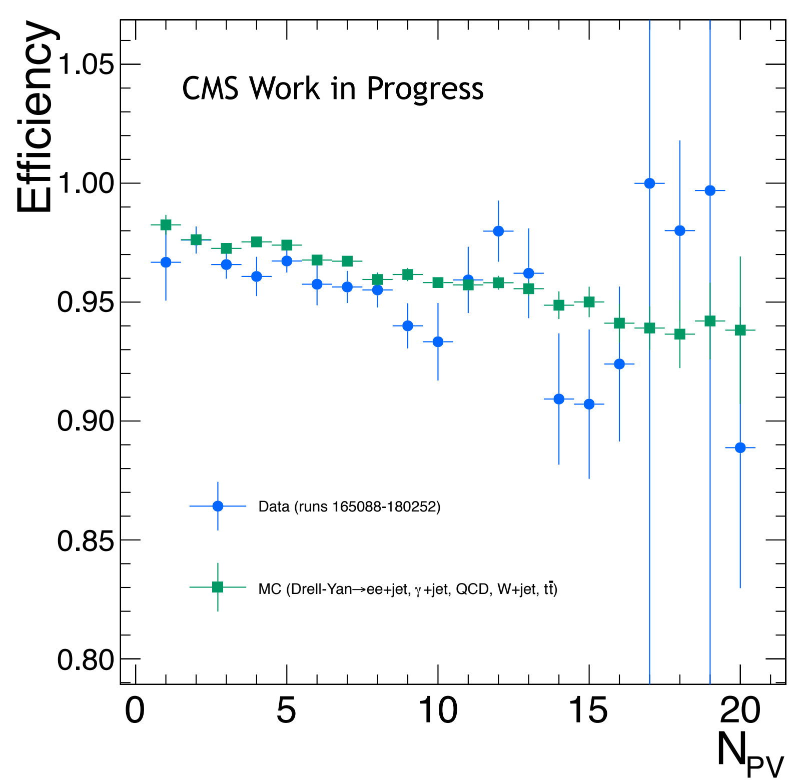

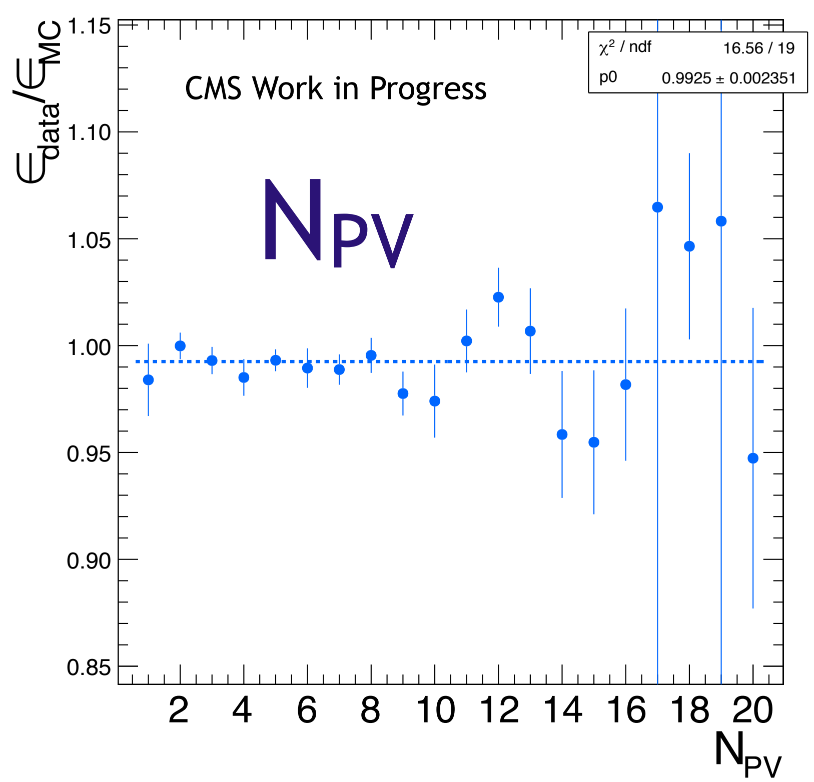

Jet selection

Variable	Cut
Algorithm	`L1FastL2L3Residual` corrected PF
p_T	> 30 GeV
$\|\eta\|$	< 2.6
Neutral hadronic energy fraction	< 0.99
Neutral electromagnetic energy fraction	< 0.99
Number of constituents	> 1
Charged hadronic energy	> 0.0 GeV if $\|\eta\| < 2.4$
Number of charged hadrons	> 0 if $\|\eta\| < 2.4$
Charged electromagnetic energy fraction	< 0.99 if $\|\eta\| < 2.4$

- ≥1 jet not overlapping any electron, photon, or fake (loosely isolated) photon

Backgrounds

- Dominant: **QCD with fake ME_T**
  - Diphoton
  - γ + jet: 1 jet misidentified as a photon
  - Multijet: at least 2 jets misidentified as photons
- Subdominant: **electroweak processes with real ME_T**
  - $W(\rightarrow e\nu)\gamma$: electron misidentified as a photon
  - $W(\rightarrow e\nu)$ + jet: electron and jet misidentified as photons

Estimating the QCD background

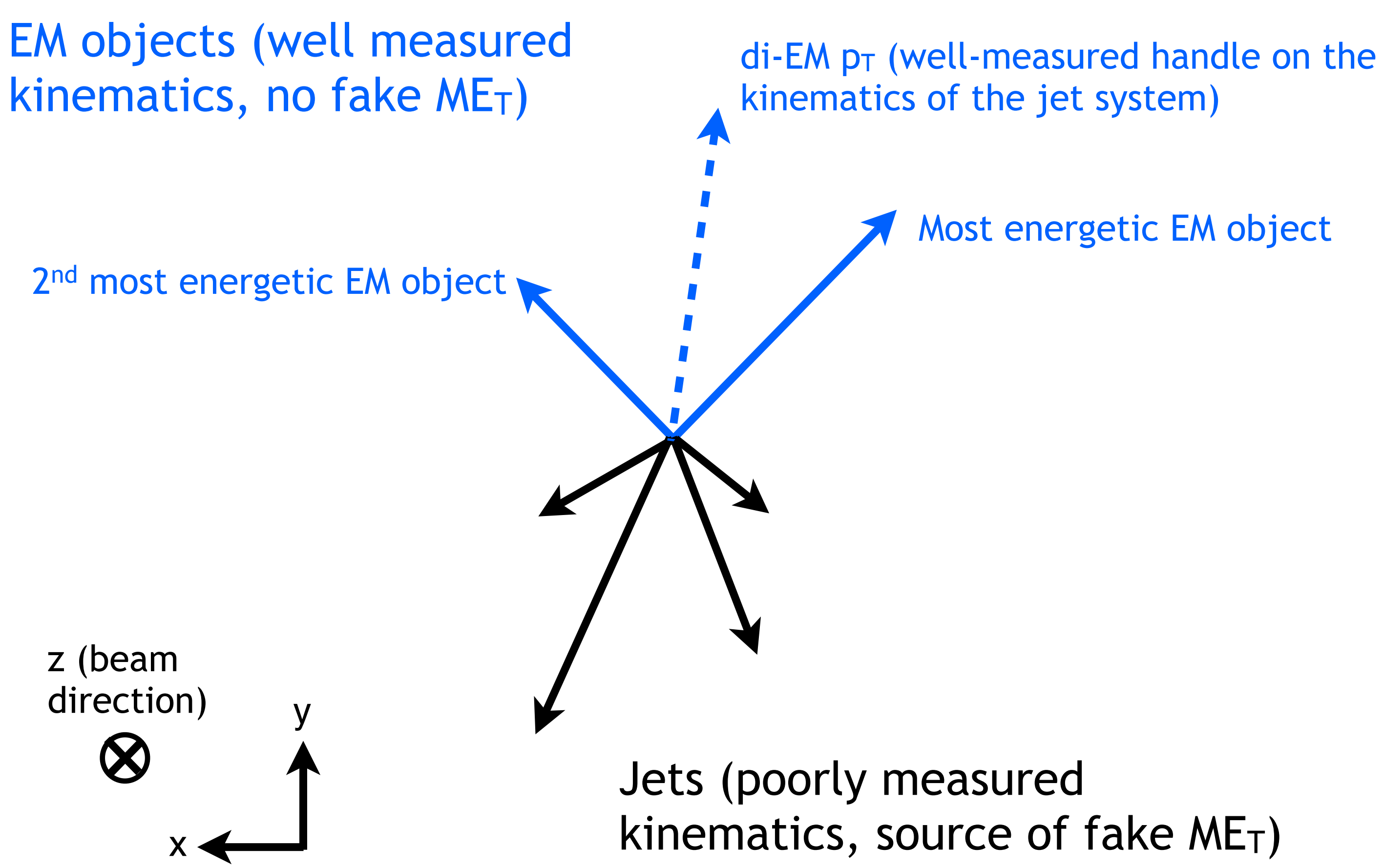

- **EM superior to hadronic energy resolution** ⇒ fake ME_T due entirely to jet mismeasurement
- **Measure QCD background from data**—control sample with well-measured EM objects to model the QCD fake ME_T spectrum
- **Reweight** events in control sample based on di-EM p_T (kinematics) and N_j (hadronic activity)
- **Normalize** the predicted QCD fake ME_T spectrum to a signal-depleted region with ME_T < 20 GeV

Reweighting

Step 1: Find a control sample similar to the $\gamma\gamma$ search sample

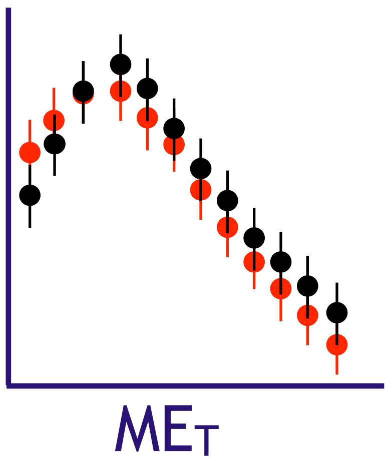

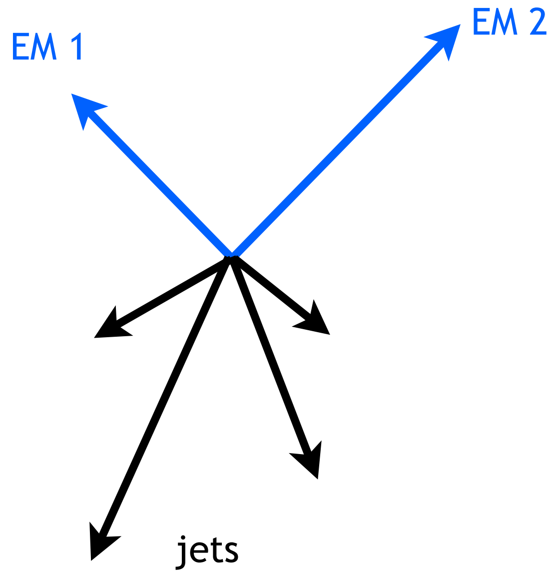

Step 2: p_T of di-EM system different between control and $\gamma\gamma$ samples $\Rightarrow$ different ME_T $\Rightarrow$ assign weight to control event based on di-EM p_T

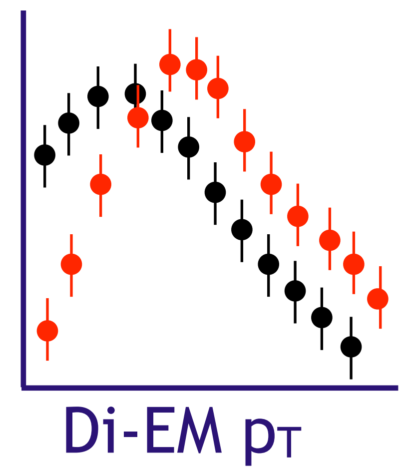

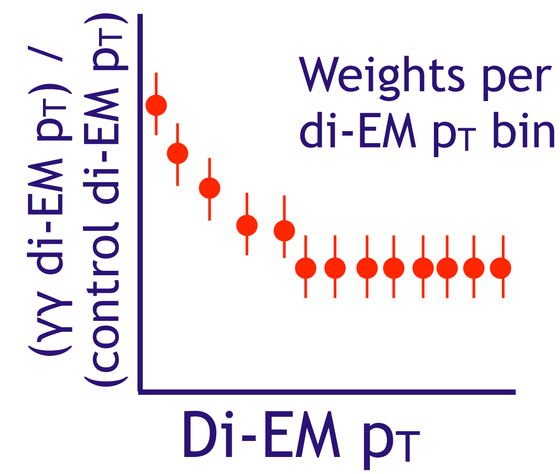

Step 3: Repeat step 2 for events with 0 jets, 1 jet, and ≥2 jets.

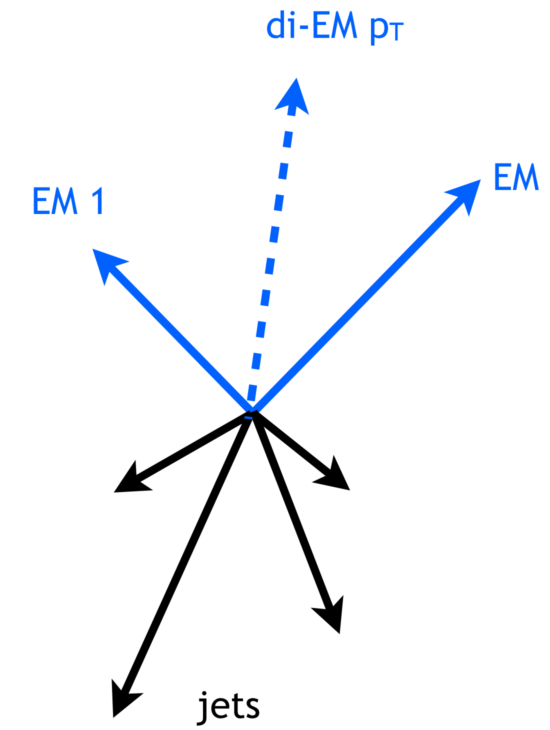

Step 4: Weight each event in control ME_T distribution with weights from steps 2-3.

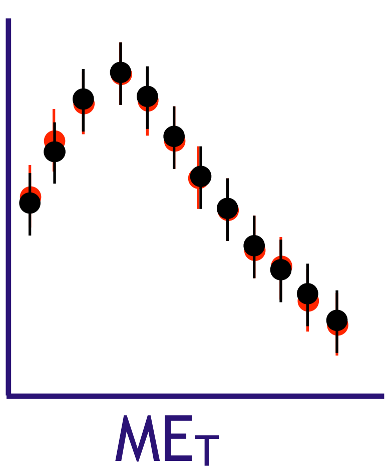

γγ sample

control sample

QCD control samples

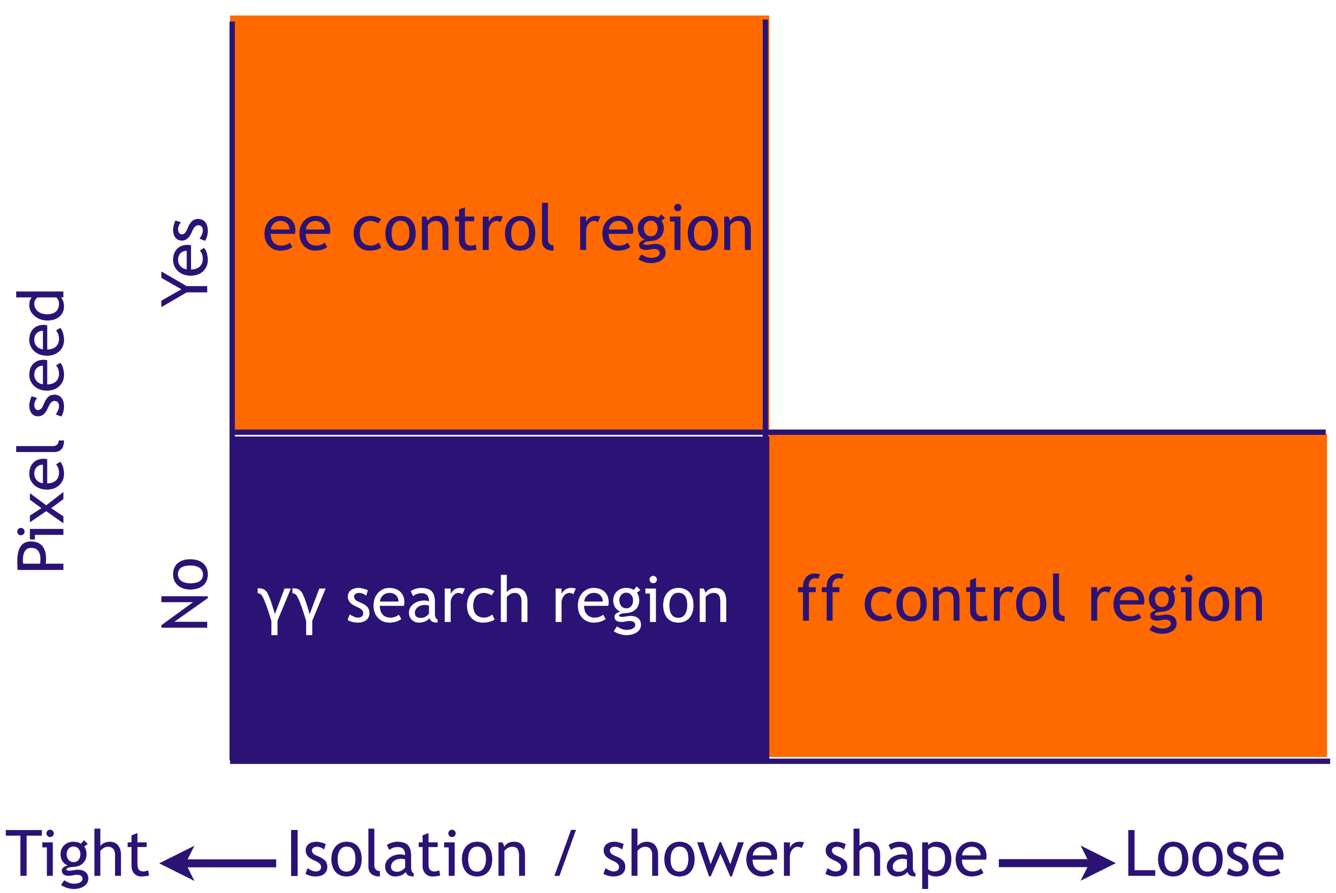

- Z dielectron (ee)
  - 81 GeV $\leq m_{ee} <$ 101 GeV
  - Photon with inverted pixel seed veto $\Rightarrow$ similar energy resolution as photons
  - Di-EM p_T reweighting significant because the kinematics of Z and QCD diphoton production are different
  - Subtract tt contribution to ee sample using invariant mass sidebands
- Electromagnetic dijets (ff)
  - Photon with inverted isolation or shower shape, below a maximum allowed isolation
  - Tends to have a little bit of HCAL energy, so use PF E_T instead of ECAL E_T
  - Similar kinematics to diphoton sample, so reweighting has small effect

Di-EM p_T spectra

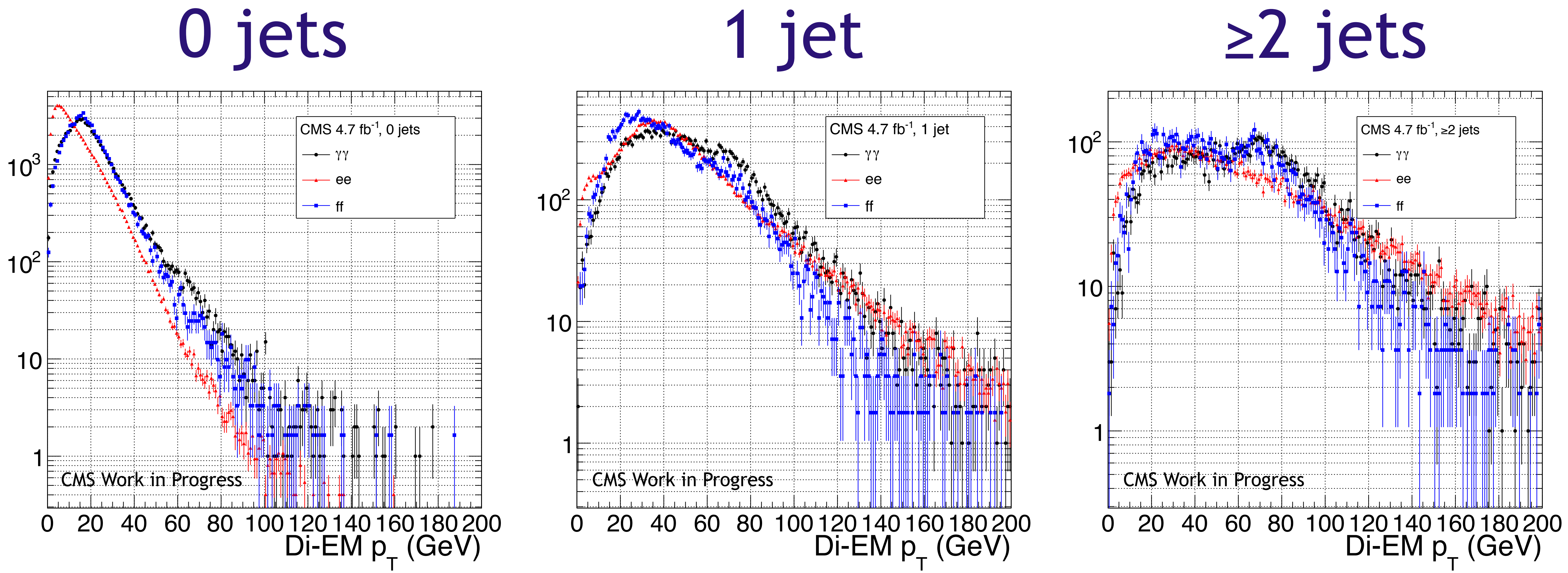

- ee (red) and ff (blue) spectra area-normalized to γγ (black) spectrum
- $w_{ij} = (N_{control}/N_{\gamma\gamma})(N_{\gamma\gamma}^{ij}/N_{control}^{ij})$
  - i runs over di-EM p_T bins
  - j runs over N_j bins

Estimating the electroweak background

eγ control region:
1 e + 1 γ

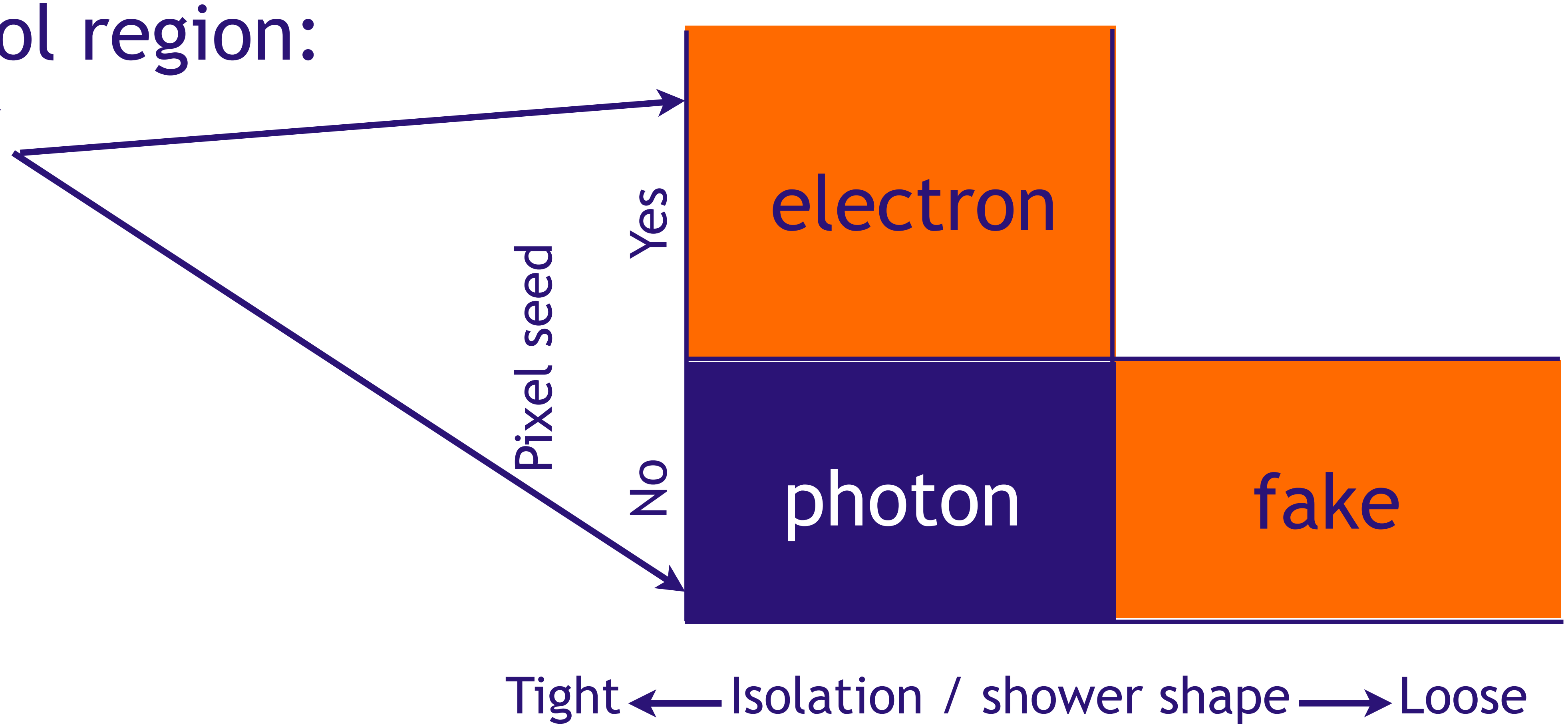

- W(→eν)γ and W(→eν) + jet can fake γγ if the electron pixel seed is missed
- Estimate the electron→photon mis-ID rate $f_{e\to\gamma}$ by fitting for the Z contribution in the ee and eγ samples
- $f_{e\to\gamma} = 0.015 \pm 0.002(\text{stat.}) \pm 0.005(\text{syst.})$
  - Systematic error due to small p_T dependence of the mis-ID rate
- Scale eγ sample by $f_{e\to\gamma}/(1 - f_{e\to\gamma})$

Results

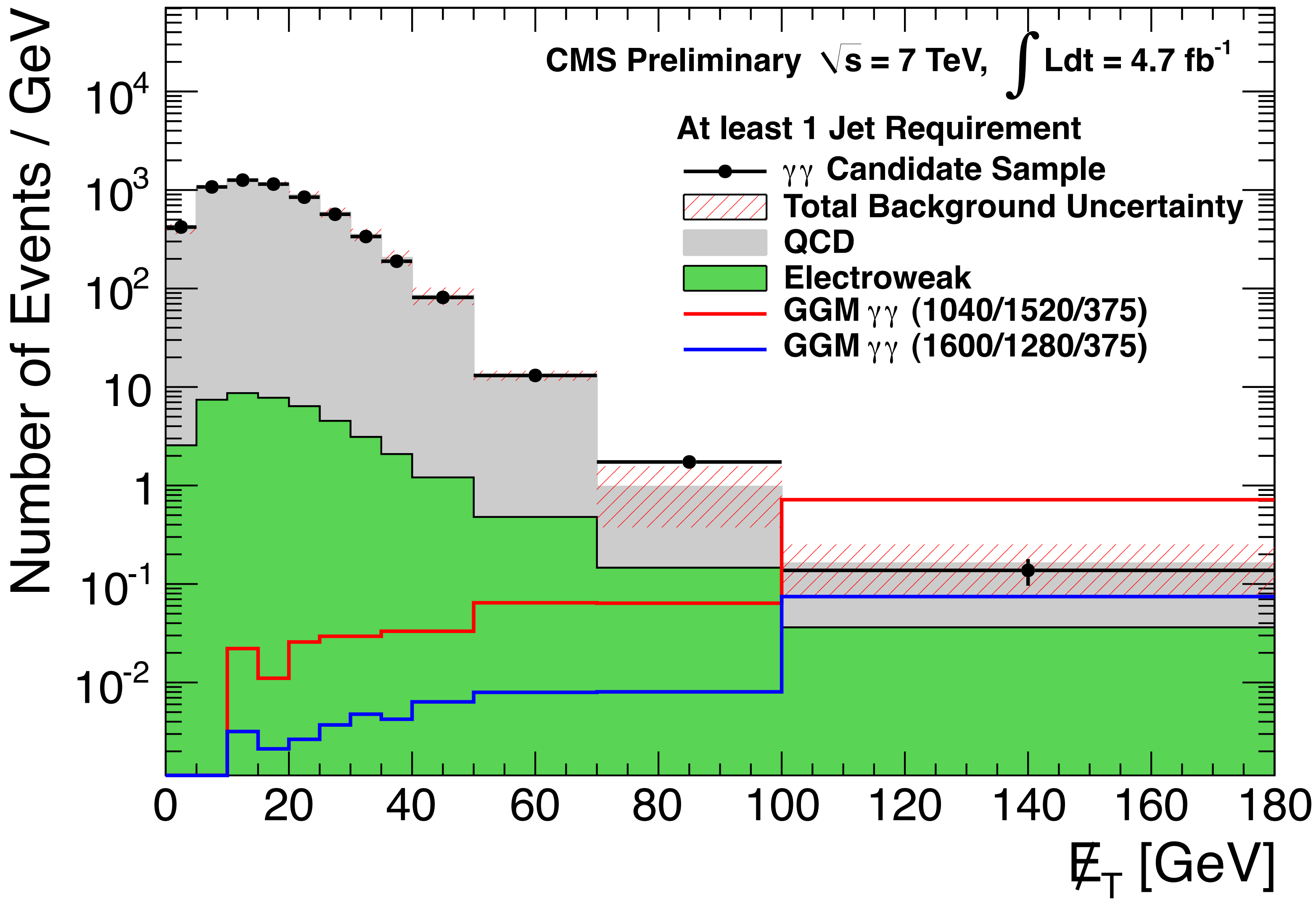

- ff sample used for the primary QCD background estimate
- Difference between ee and ff prediction taken as a systematic error
- Use ME_T > 50 GeV as search region

Upper limit calculation

- CL_S 95%
- Limits calculated in multiple ME_T bins and then combined
  - 50-60 GeV, 60-80 GeV, 80-100 GeV, 100-140 GeV, 140-180 GeV, and ≥180 GeV
- Uncertainties on signal acceptance × efficiency, background, and integrated luminosity modeled with log-normal distributions

Source	Systematic uncertainty (%)
Integrated luminosity	4.5
Background estimate	~48
Statistics	~32
Reweighting	~2.3
Normalization	~0.23
Electron→photon mis-ID rate	31
Difference between ff and ee	~35
Acceptance × efficiency	7-72
Photon ID efficiency correction	4
PDF error on cross section	4-66
PDF error on acceptance	0.1-9
Renormalization scale	4-28

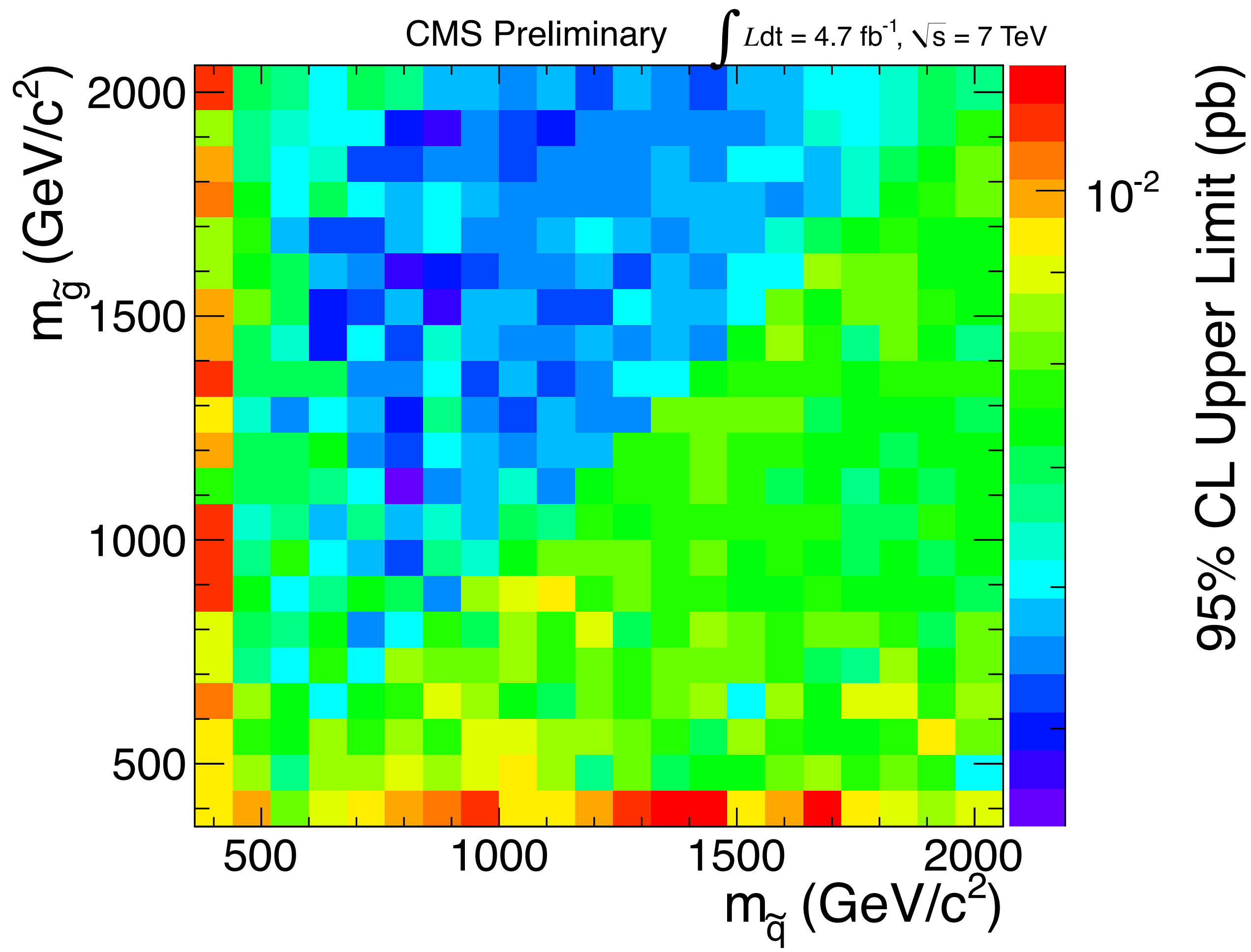

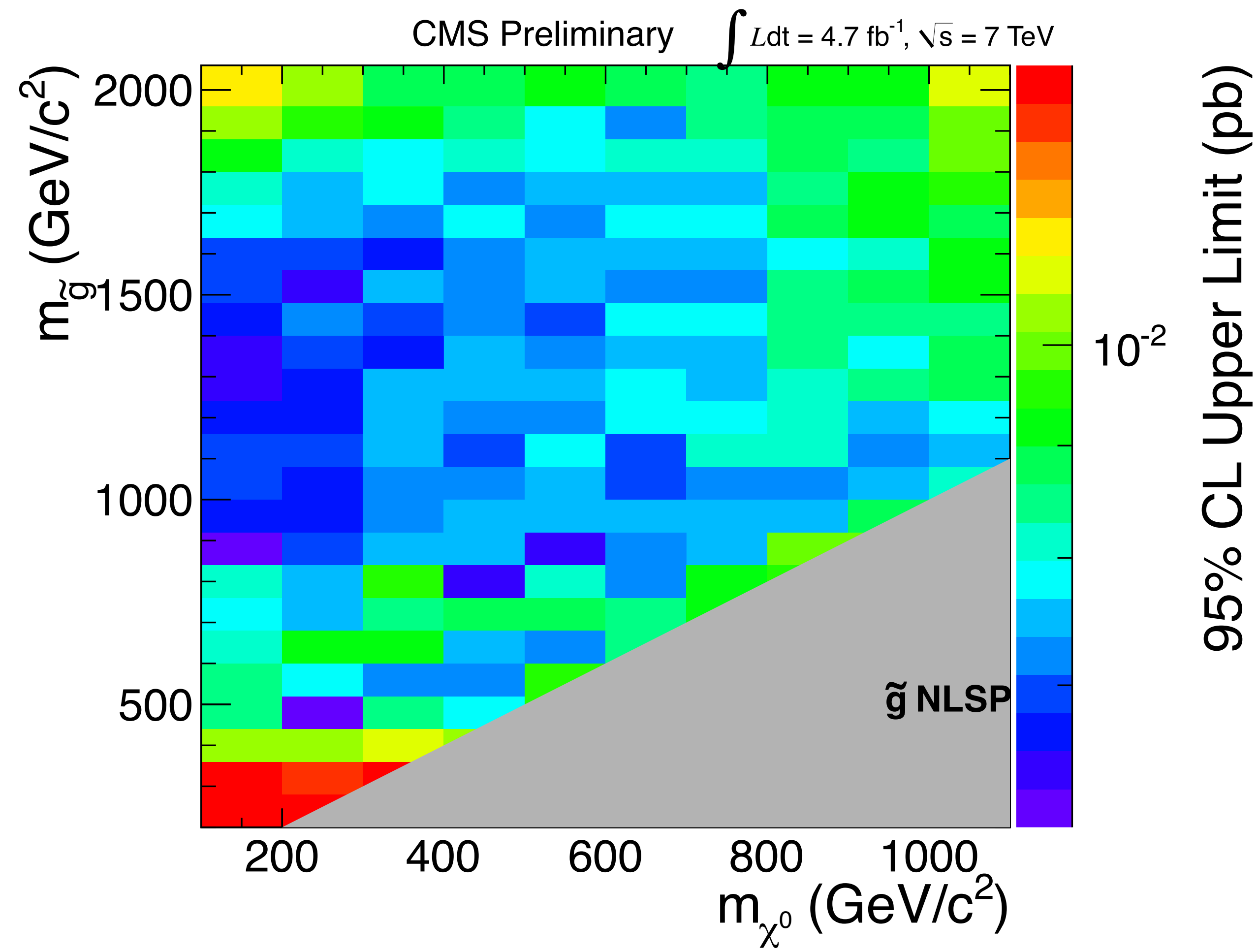

M_2 decoupled, $m_{neutralino}$ = 375 GeV, m_{gluino} vs. m_{squark}

Light squarks decoupled, m_{gluino} vs. $m_{neutralino}$

Model exclusions

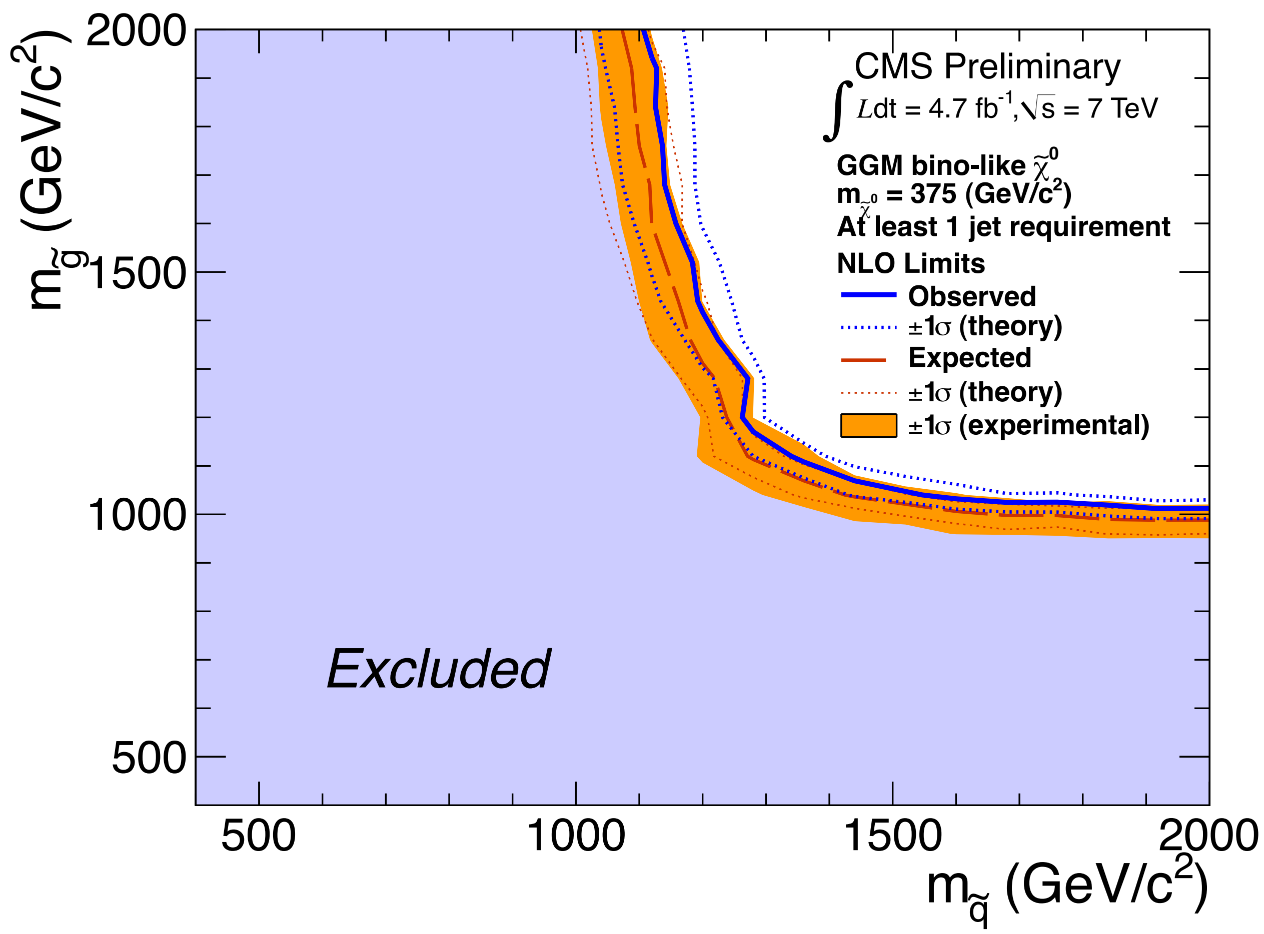

M_2 decoupled, $m_{neutralino}$ = 375 GeV, m_{gluino} vs. m_{squark}

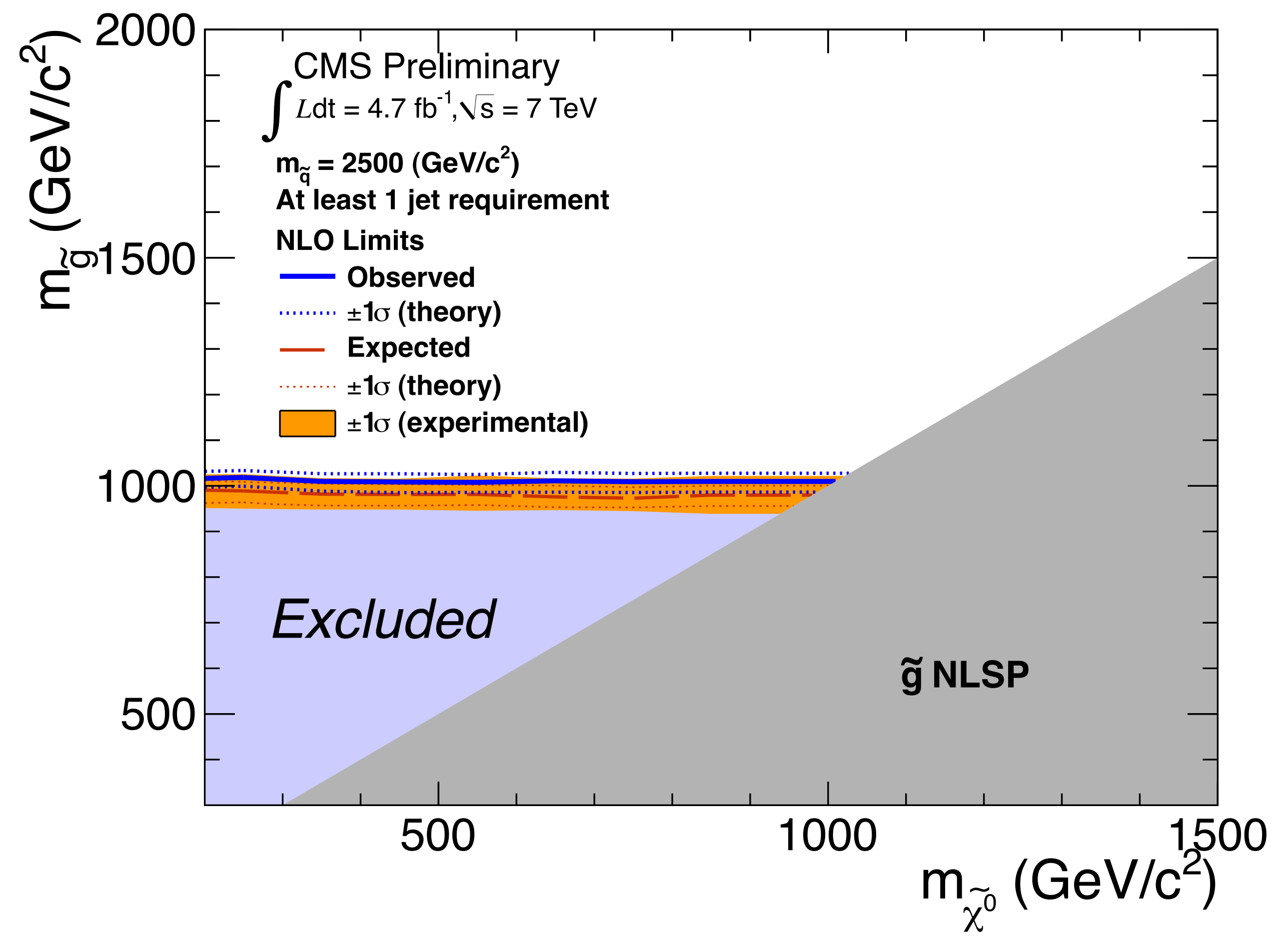

Light squarks decoupled, m_{gluino} vs. $m_{neutralino}$

Conclusions

- Top performing ECAL is an important instrument in the quest for new physics at CMS
  - Steadily moving toward design calibration precision
  - Utilized in Higgs, SUSY, and Exotica searches
- Searches in the diphoton final state are powerful tools for observing SUSY
  - Clean trigger objects
  - Dominant background estimated from data
- 4.7 fb^{-1} search has excluded gluinos and light squarks in the GMSB scenario below ~1 TeV
  - Best exclusions to date on gauge mediation
  - As energy and luminosity increase, different variants on the diphoton search can be explored to give the best coverage of possible SUSY scenarios
- Looking forward to 2012!

Backup

ECAL performance

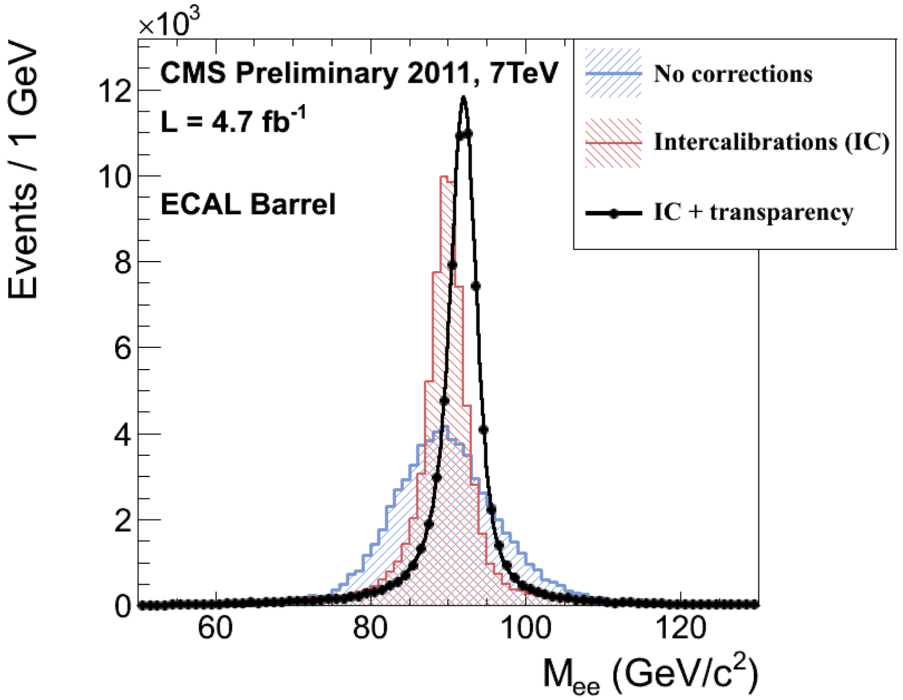

[3]

Effect of intercalibration and transparency corrections on the Z→ee mass peak position and width

W relative E/p vs. time

[3]

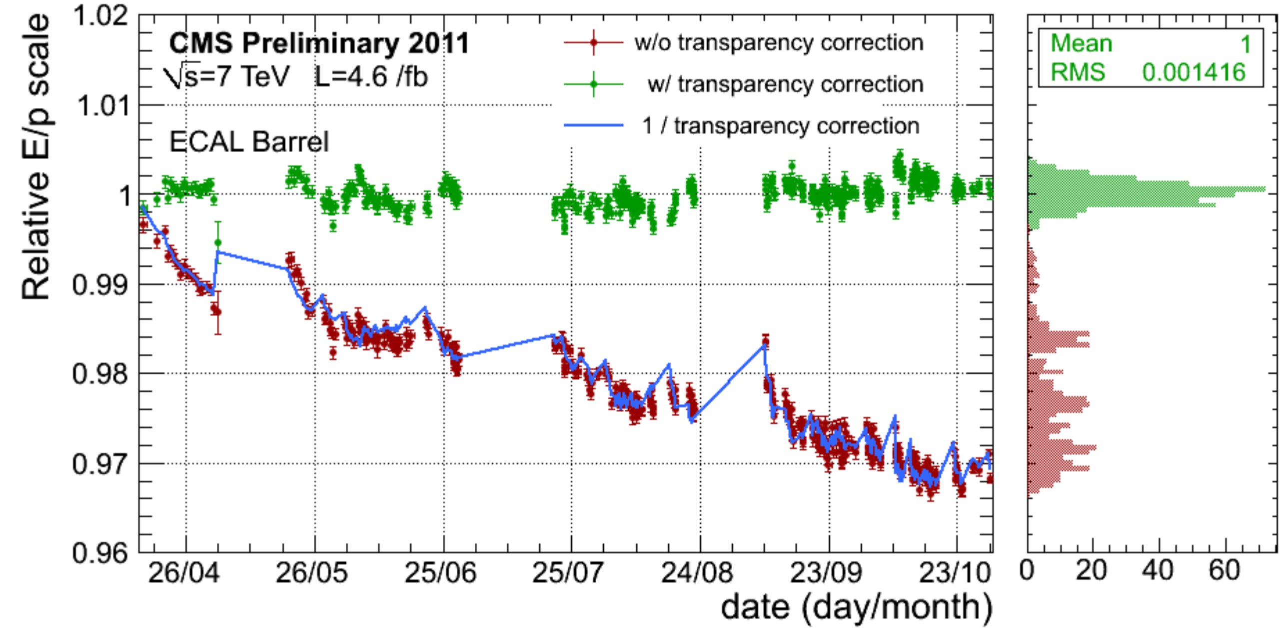

[10]

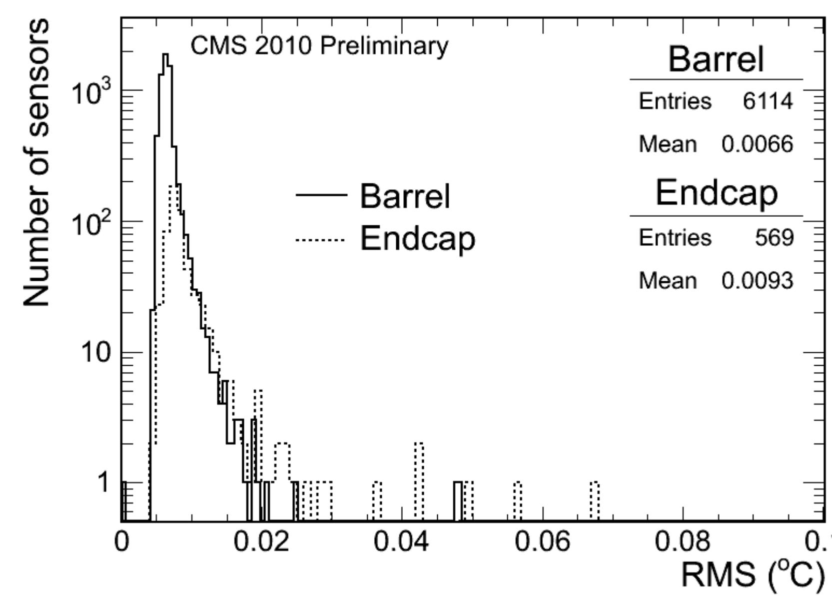

June 2010 - Dec 2010

RMS deviation of supercrystal temperature measurements over 2010 running

Comparison of crystal properties

[2]

	NaI(Tl)	BGO	CSI	BaF_2	CeF_3	$PbWO_4$
Density [g/cm^3]	3.67	7.13	4.51	4.88	6.16	8.28
Radiation length [cm]	2.59	1.12	1.85	2.06	1.68	0.89
Interaction length [cm]	41.4	21.8	37.0	29.9	26.2	22.4
Molière radius [cm]	4.80	2.33	3.50	3.39	2.63	2.19
Light decay time [ns]	230	60 300	16	0.9 630	8 25	5 (39%) 15 (60%) 100 (1%)
Refractive index	1.85	2.15	1.80	1.49	1.62	2.30
Maximum of emission [nm]	410	480	315	210 310	300 340	440
Temperature coefficient [%/°C]	~0	–1.6	–0.6	–2/0	0.14	–2
Relative light output	100	18	20	20/4	8	1.3

Expected radiation dose

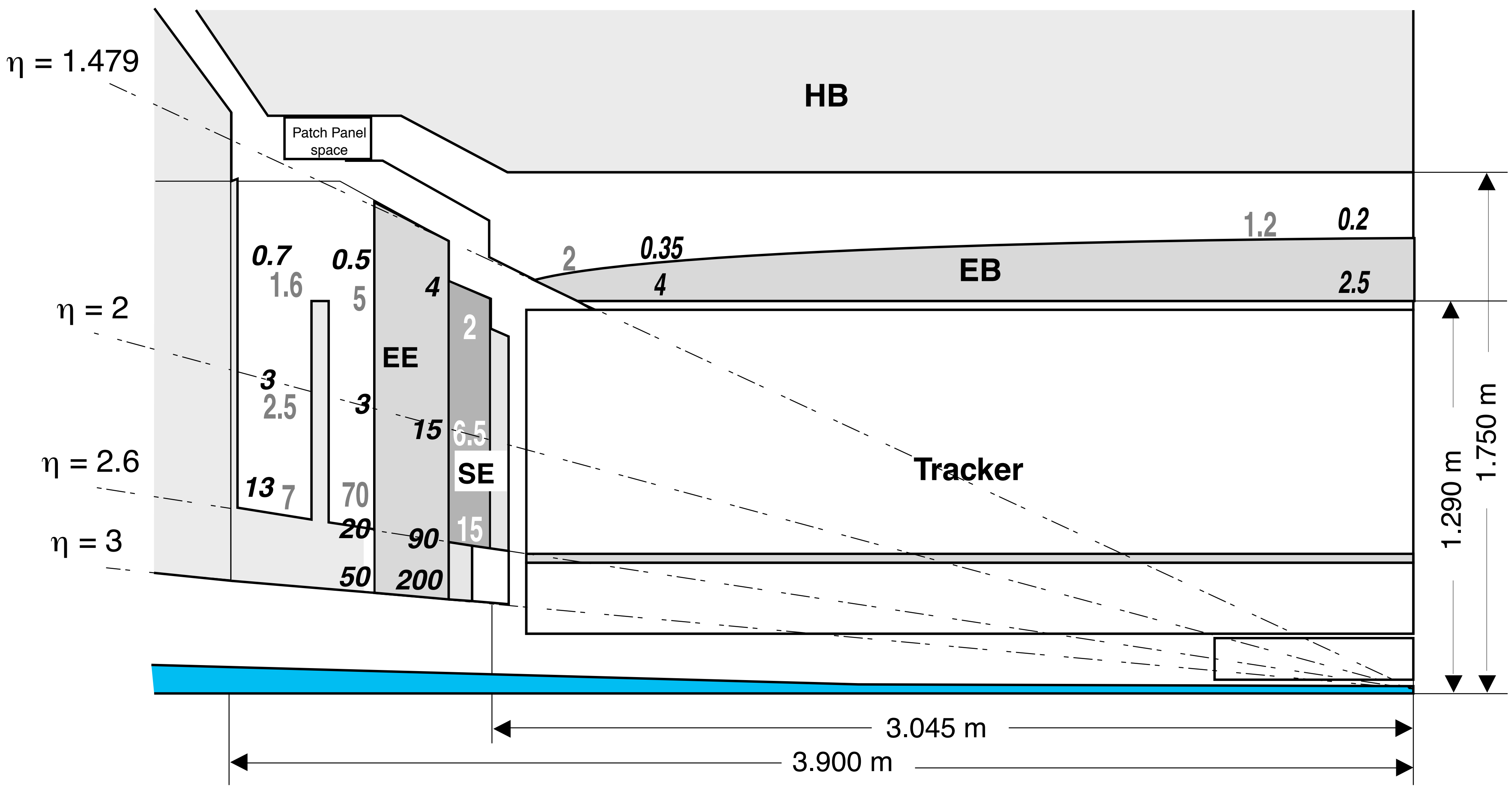

[2]

Fig. 1.4: The dose and neutron fluence in and around the crystals as a function of pseudorapidity. Numbers in bold italics are doses, in kGy, at shower maximum and at the rear of the crystals. The other numbers are fluences immediately behind the crystals, in the space for endcap electronics surrounded by moderators and in the silicon of the preshower in units of 10^{13} cm^{-2}. All values correspond to an integrated luminosity of 5×10^5 pb^{-1} appropriate for the first ten years of LHC operation.

Previous VPT rate effect

[16]

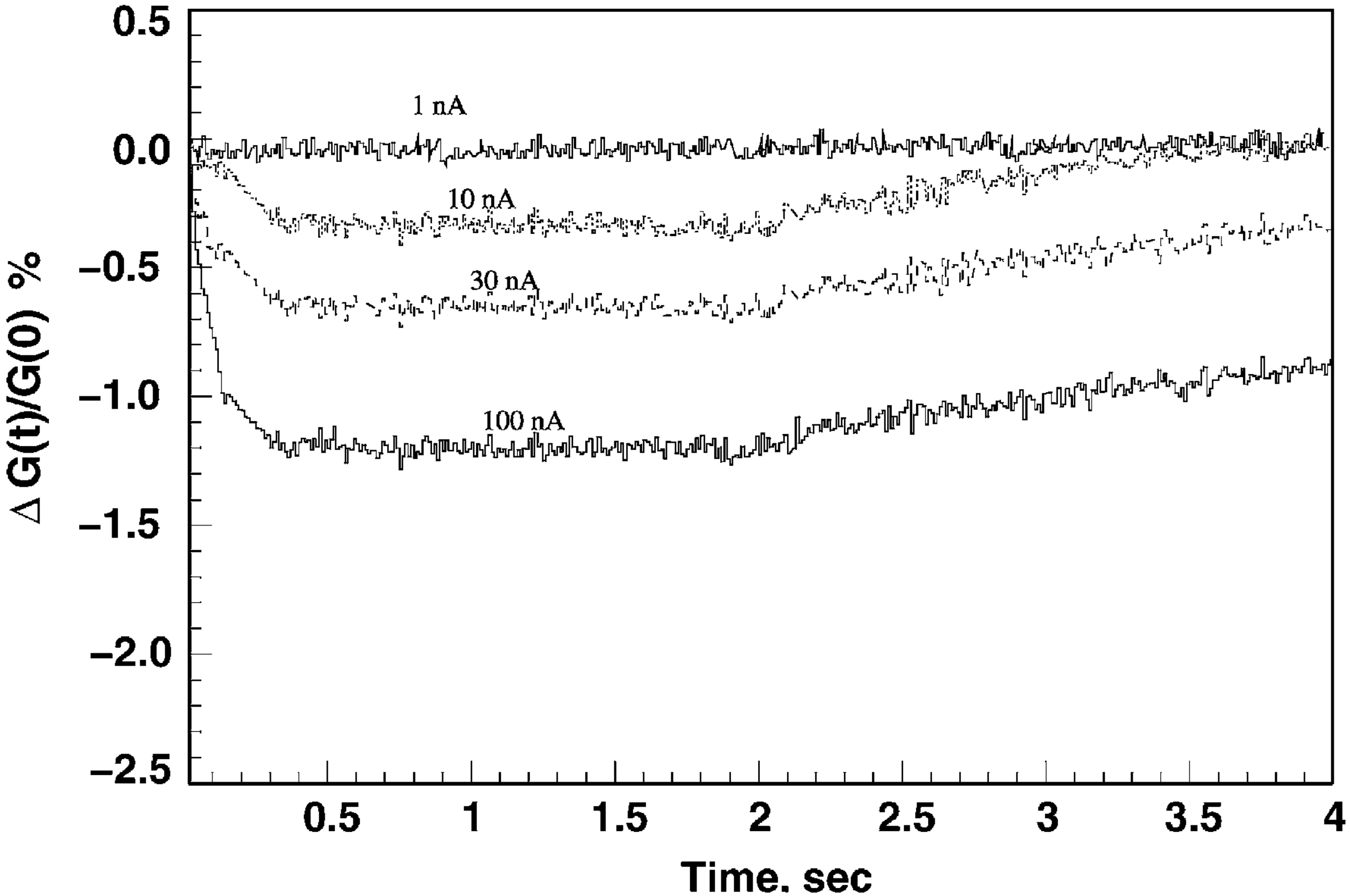

Fig. 5. Relative variation of the VPT gain averaged over 20 spills as a function of time for different average VPT anode currents.

LED running modes

- Calibration sequence
  - Few hundred LED pulses read out (readout rate ~100 Hz) for each EE monitoring region
  - Continuous monitoring of the VPTs and crystals, to complement the laser monitoring
- Local run
  - Short sequence of a few hundred LED pulses triggered by ECAL-generated trigger and read out
  - Useful for debugging the system and checking the health of the ECAL
- Soaking
  - Fire the blue LED stability pulses all the time in the abort gaps to dampen VPT gain changes
  - Frequency up to ~11.4 kHz (use only 100 Hz right now)

Flavor blindness of GMSB

- SUSY must be a broken symmetry — if not, each SM particle and its superpartner would have the same mass, and the superpartners would have been discovered already

- SUSY-breaking terms in the minimal SUSY Lagrangian generically allow for lepton flavor violating decays:

$$\begin{aligned}
\mathcal{L}_{\rm soft}^{\rm MSSM} = & -\frac{1}{2}\left(M_3 \tilde{g}\tilde{g} + M_2 \widetilde{W}\widetilde{W} + M_1 \widetilde{B}\widetilde{B} + {\rm c.c.}\right) \\
& - \left(\tilde{\bar{u}}\,\mathbf{a_u}\,\tilde{Q}H_u - \tilde{\bar{d}}\,\mathbf{a_d}\,\tilde{Q}H_d - \tilde{\bar{e}}\,\mathbf{a_e}\,\tilde{L}H_d + {\rm c.c.}\right) \\
& - \tilde{Q}^\dagger\,\mathbf{m_Q^2}\,\tilde{Q} - \tilde{L}^\dagger\,\mathbf{m_L^2}\,\tilde{L} - \tilde{\bar{u}}\,\mathbf{m_{\bar{u}}^2}\,\tilde{\bar{u}}^\dagger - \tilde{\bar{d}}\,\mathbf{m_{\bar{d}}^2}\,\tilde{\bar{d}}^\dagger \boxed{- \tilde{\bar{e}}\,\mathbf{m_{\bar{e}}^2}\,\tilde{\bar{e}}^\dagger} \\
& - m_{H_u}^2 H_u^* H_u - m_{H_d}^2 H_d^* H_d - (bH_uH_d + {\rm c.c.})\,.
\end{aligned}$$

$$\begin{bmatrix} \widetilde{e}_R \\ \widetilde{\mu}_R \\ \widetilde{\tau}_R \end{bmatrix} \begin{bmatrix} c_{ee} & c_{e\mu} & c_{e\tau} \\ c_{\mu e} & c_{\mu\mu} & c_{\mu\tau} \\ c_{\tau e} & c_{\tau\mu} & c_{\tau\tau} \end{bmatrix} \begin{bmatrix} \widetilde{e}_R & \widetilde{\mu}_R & \widetilde{\tau}_R \end{bmatrix}$$

if not proportional to the unit matrix, will lead to, for example, $\mu \to e\gamma$

- The relation $c_{ee} = c_{\mu\mu} = c_{\tau\tau} = m^2$ (and similar for the other fermion families) arises naturally in GMSB, because the sparticle masses (i.e. the diagonal terms) only depend on their gauge couplings, which are identical for the three families

GMSB searches with photons

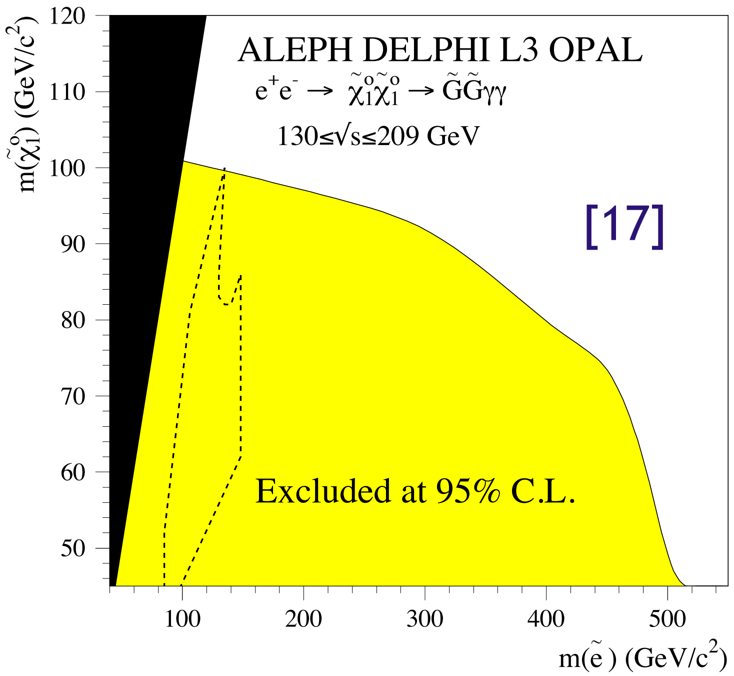

LEP (1989-2000)

- Minimal GMSB model
- Neutralino pair production
- $m_{neutralino}$ > 97 GeV for short-lived neutralino

Tevatron Run II (2001-2010)

- Minimal GMSB model (SPS8) [18]
- Chargino and neutralino pair production
- $m_{neutralino}$ > ~170 GeV (Λ > 124 TeV) for short-lived neutralino

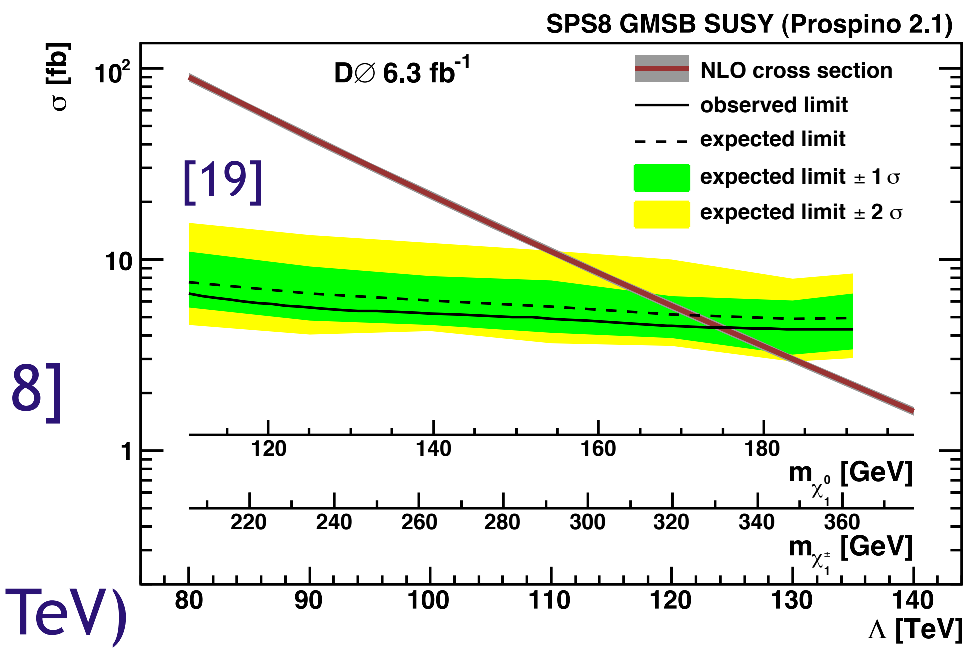

LHC7 (2009-2011)

- Simplified model parametrized in terms of tan β and squark, gluino, and wino/bino/higgsino masses
- No assumptions on the number of messengers, the messenger mass, or the SUSY breaking scale
- Squark and gluino production
- Short-lived neutralino

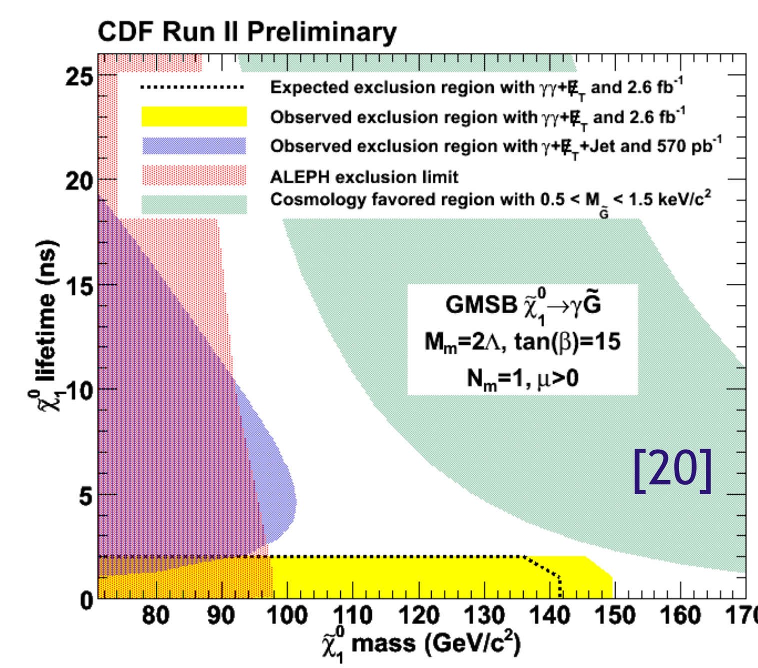

CMS longitudinal cross section

[2]

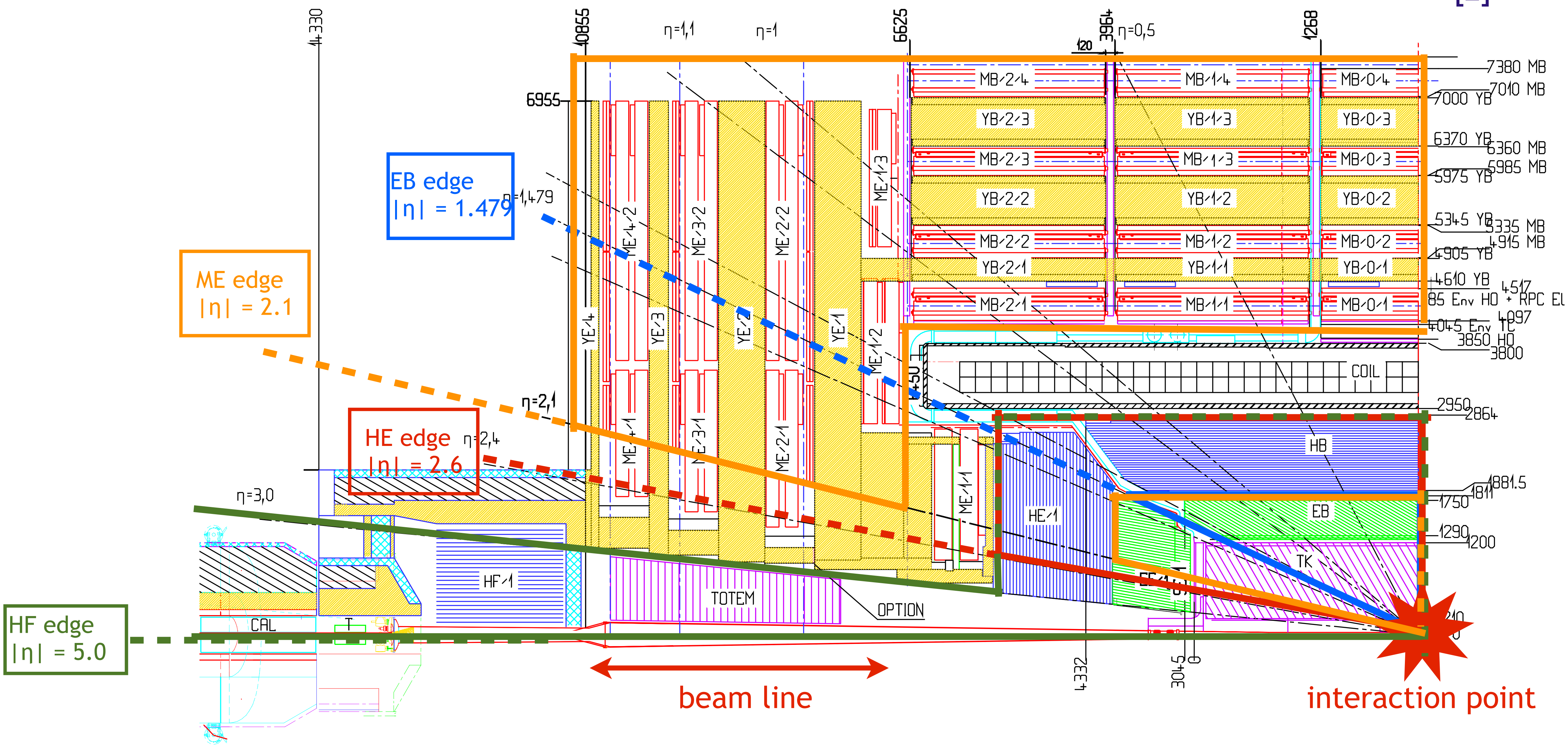

Trigger definitions

- IsoVL
  - $I_{ECAL} < 0.012E_T + 6$ GeV
  - $I_{HCAL} < 0.005E_T + 4$ GeV
  - $I_{track} < 0.002E_T + 4$ GeV
- R9Id
  - $R9 > 0.85$

Photon isolation criteria

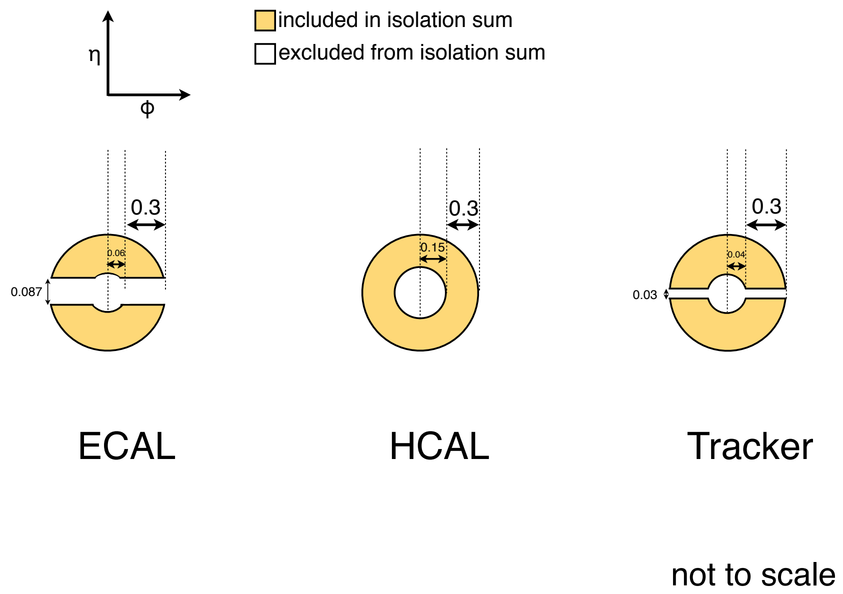

- $I_{ECAL} - 0.0792\rho + I_{HCAL} - 0.0252\rho + I_{track} < 6$ GeV
- ρ = average energy density per unit area in the calorimeters as measured by Fastjet

$$\frac{\text{HCAL energy in } R < 0.15 \text{ cone around photon candidate}}{\text{ECAL energy of photon candidate}} < 0.05$$

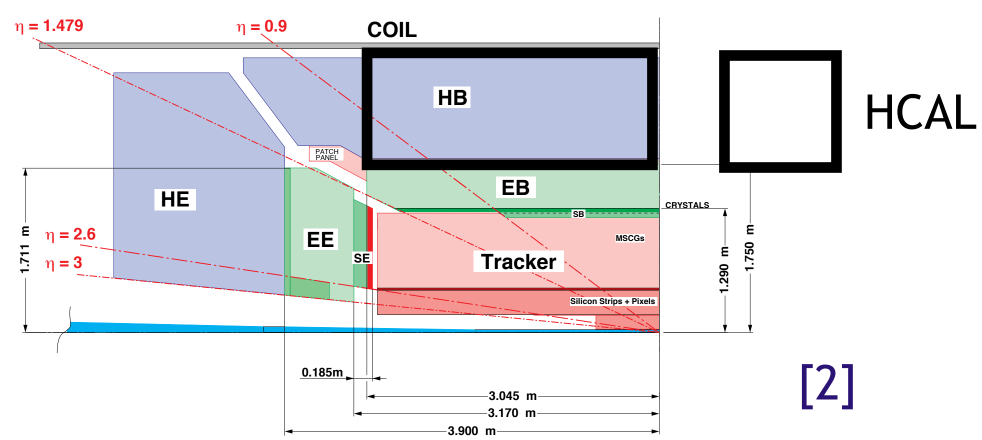

[2]

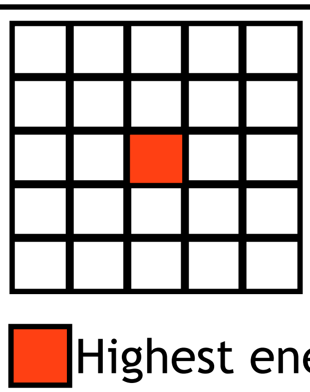

Highest energy (photon seed) crystal

$$\sigma^2_{\eta\eta} = \sum_{i=1}^{25} w_i(\eta_i - \bar{\eta})^2 / \sum_{i=1}^{25} w_i, \quad < 0.011$$

where $w_i = \max(0, 4.7 + \ln(E_i/E))$, E_i is the energy of the i^{th} crystal in a group of 5×5 centred on the one with the highest energy, and $\eta_i = \hat{\eta}_i \times \delta\eta$, where $\hat{\eta}_i$ is the η index of the ith crystal and $\delta\eta = 0.0174$; E is the total energy of the group and $\bar{\eta}$ the average η weighted by w_i in the same group [20]. [21]

ECAL noise cleaning

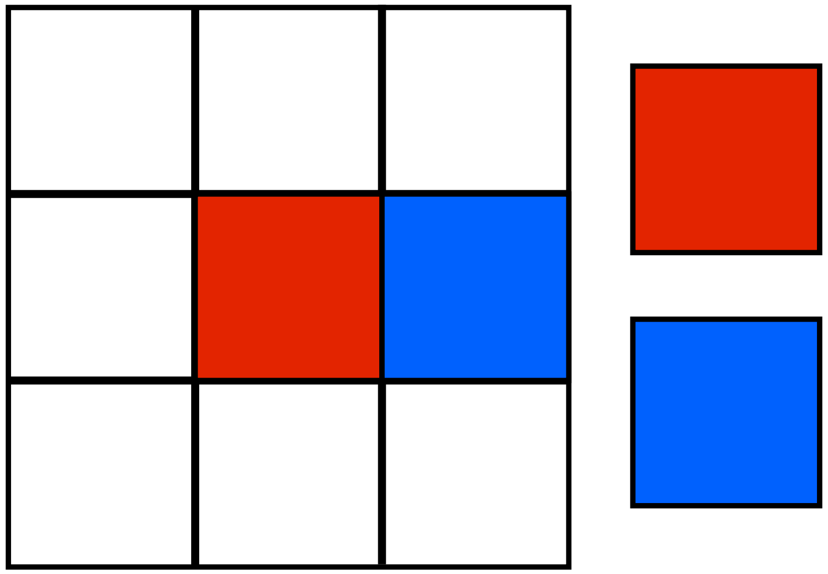

$$\frac{E_{\blacksquare} + E_{\blacksquare}}{E_{3\times 3}} > 0.95 \Rightarrow \text{reject}$$

- Form 3 × 3 matrix of crystals around the photon seed crystal
- Find the 2 highest energy crystals within the matrix
- If the sum of the energies of the 2 highest energy crystals divided by the sum of the energies of all 9 crystals within the matrix exceeds 0.95, reject the photon as ECAL noise

Photon ID variables

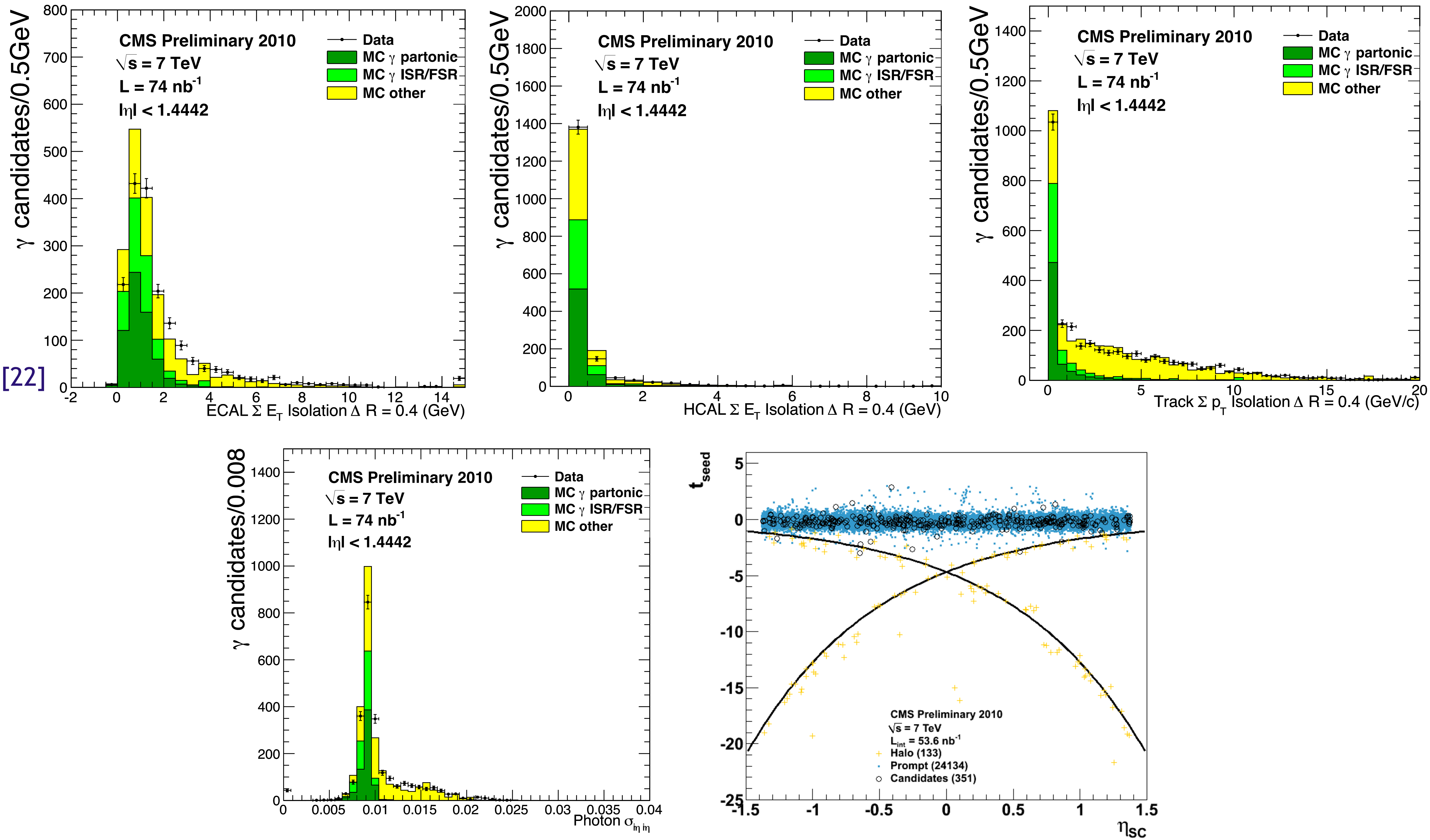

[22]

Sample definitions

Variable	Cut			
	$\gamma\gamma$	$e\gamma$	ee	ff
HLT match	IsoVL	IsoVL	IsoVL	IsoVL || R9Id
E_T	$> 40/$ > 25 GeV	$> 40/$ > 25 GeV	$> 40/$ > 25 GeV	$> 40/$ > 25 GeV
SC $\|\eta\|$	< 1.4442	< 1.4442	< 1.4442	< 1.4442
H/E	< 0.05	< 0.05	< 0.05	< 0.05
$R9$	< 1	< 1	< 1	< 1
Pixel seed	No/No	Yes/No	Yes/Yes	No/No
I_{comb}, $\sigma_{i\eta i\eta}$	< 6 GeV && < 0.011	< 6 GeV && < 0.011	< 6 GeV && < 0.011	< 20 GeV && (≥ 6 GeV || ≥ 0.011)
JSON	Yes	Yes	Yes	Yes
No. good PVs	≥ 1	≥ 1	≥ 1	≥ 1
ΔR_{EM}	> 0.6	> 0.6	> 0.6	> 0.6
$\Delta\phi_{\mathrm{EM}}$	≥ 0.05	≥ 0.05	≥ 0.05	≥ 0.05

Effect of reweighting

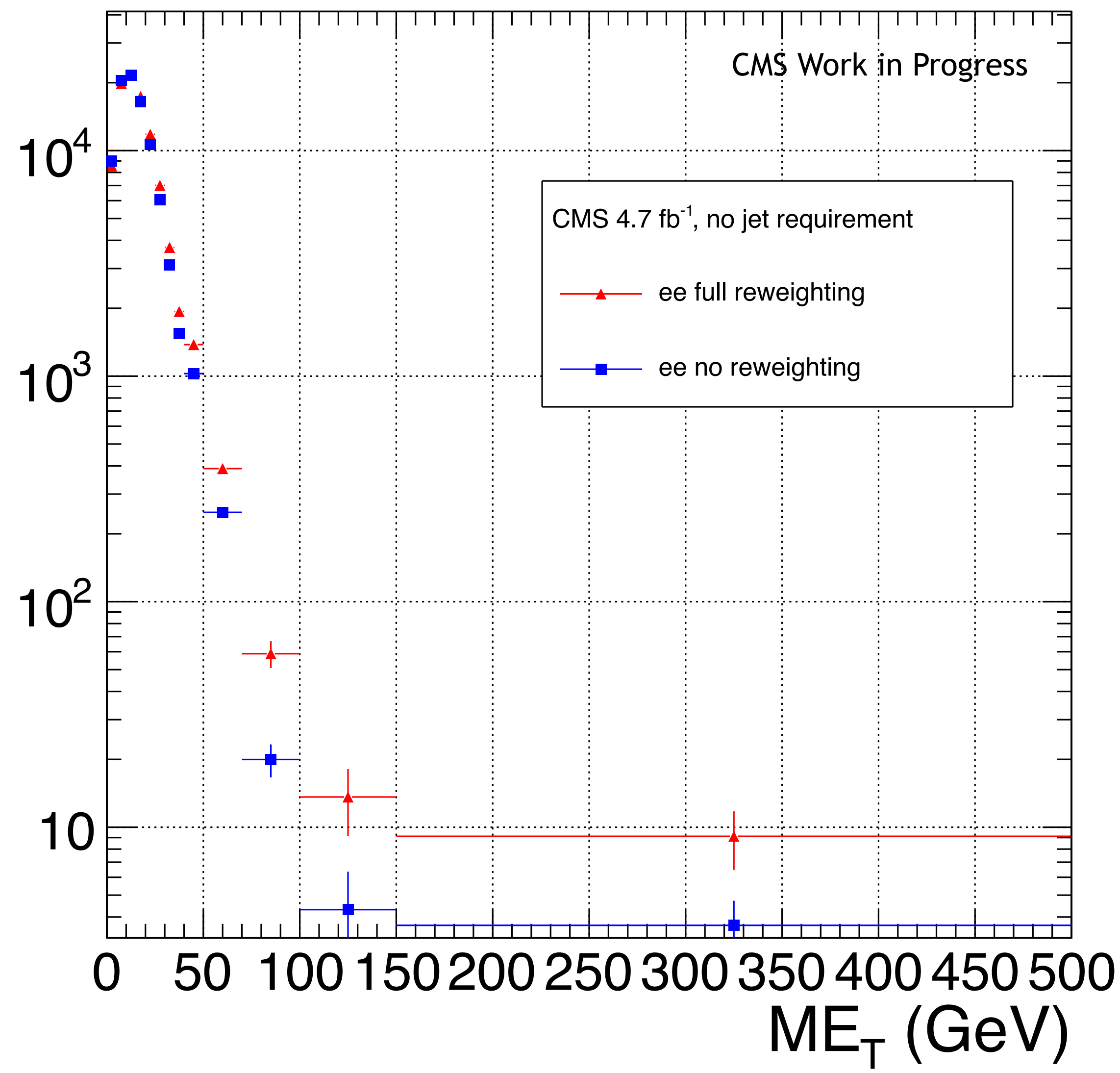

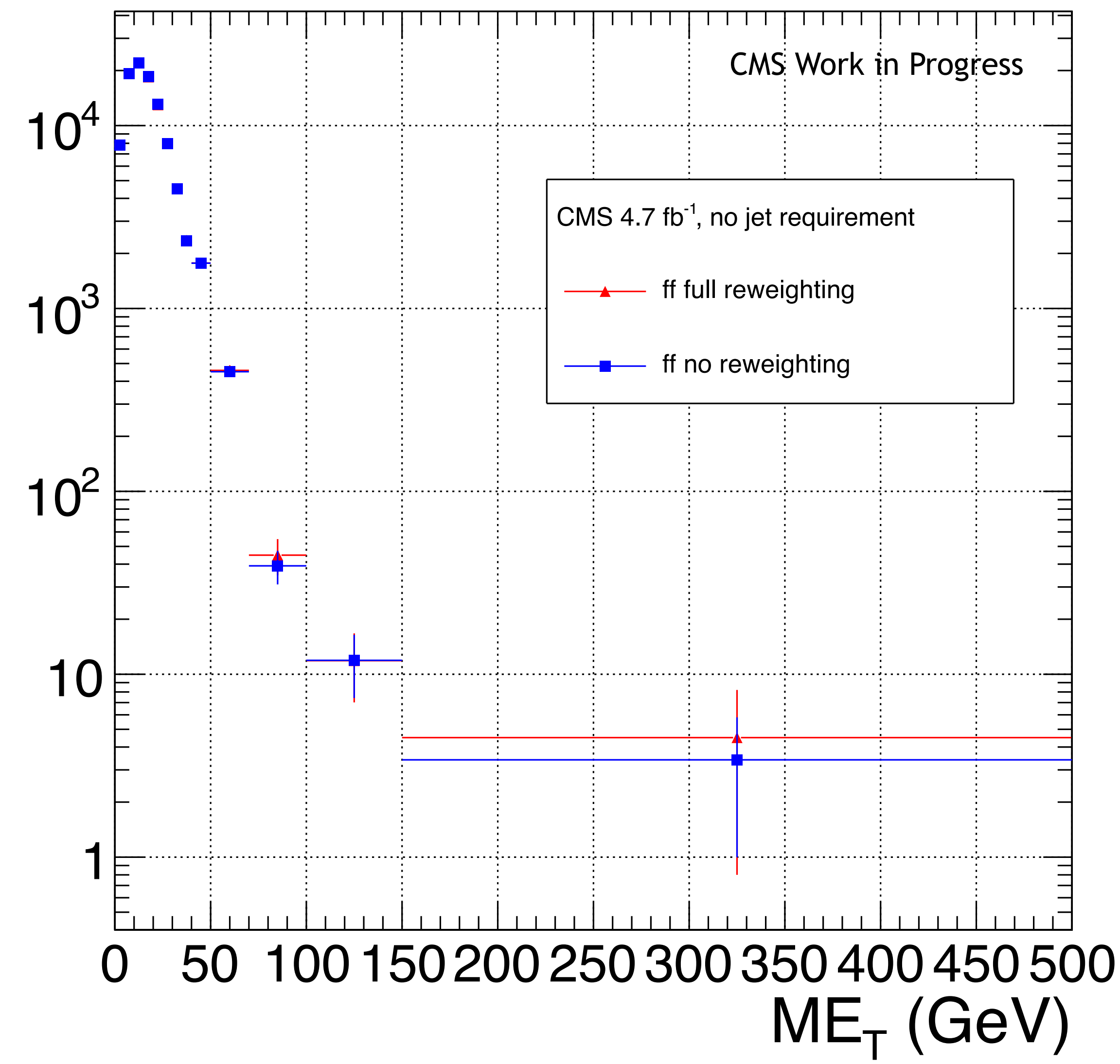

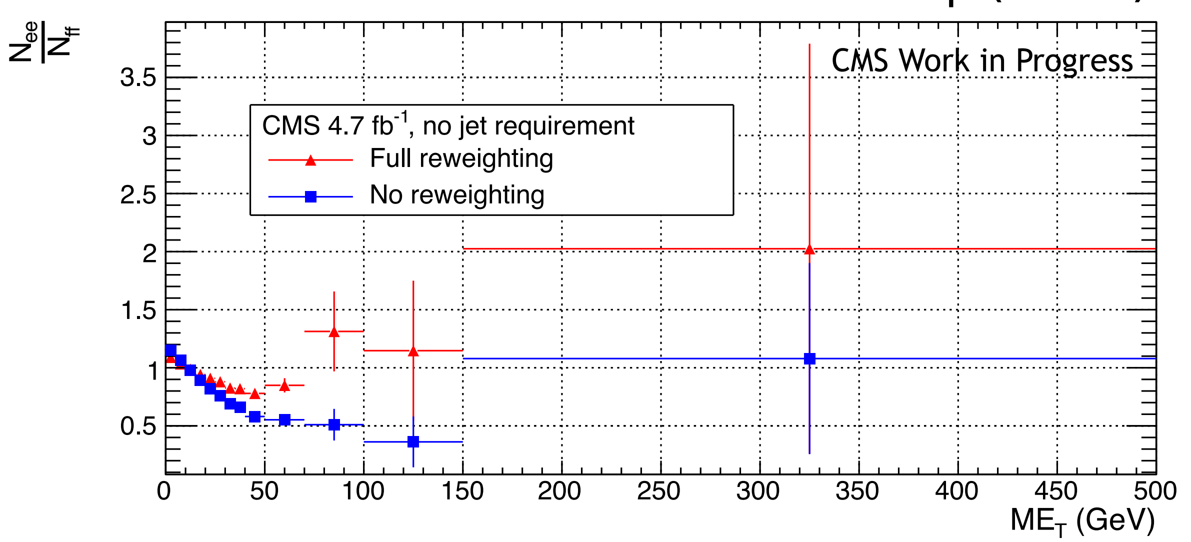

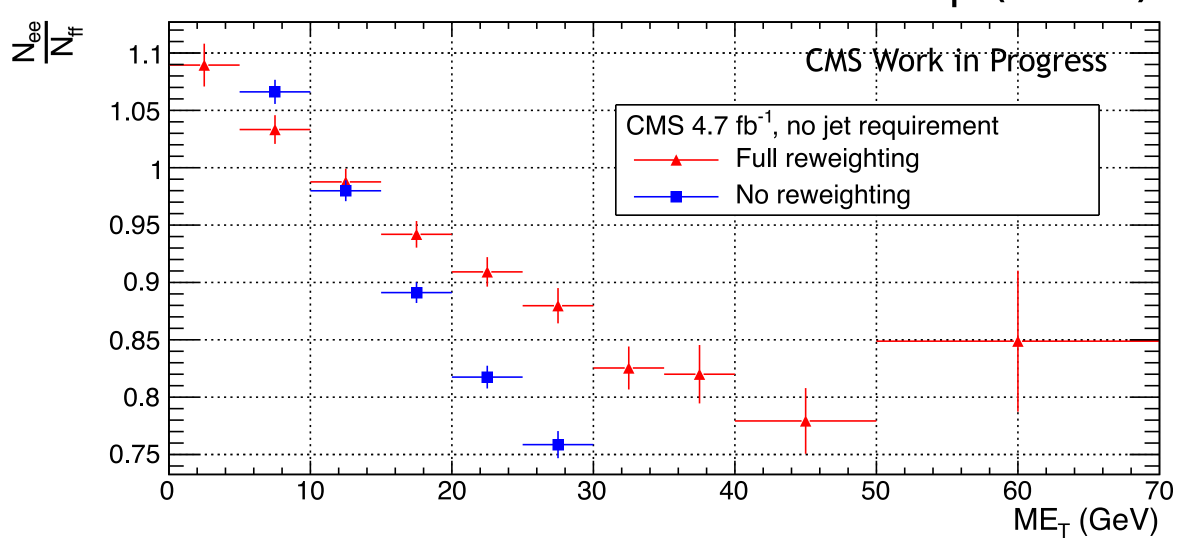

PF vs. ECAL E_T (1)

Leading e

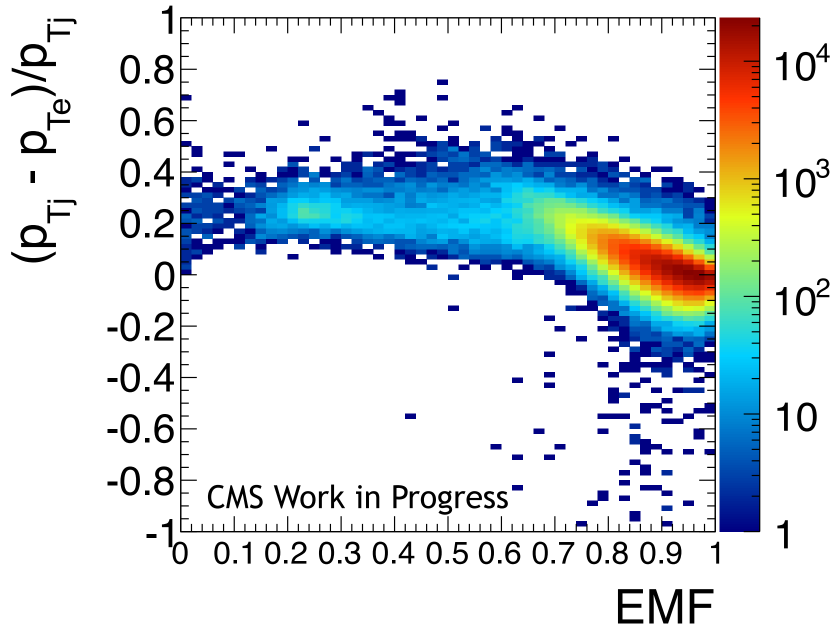

Leading f

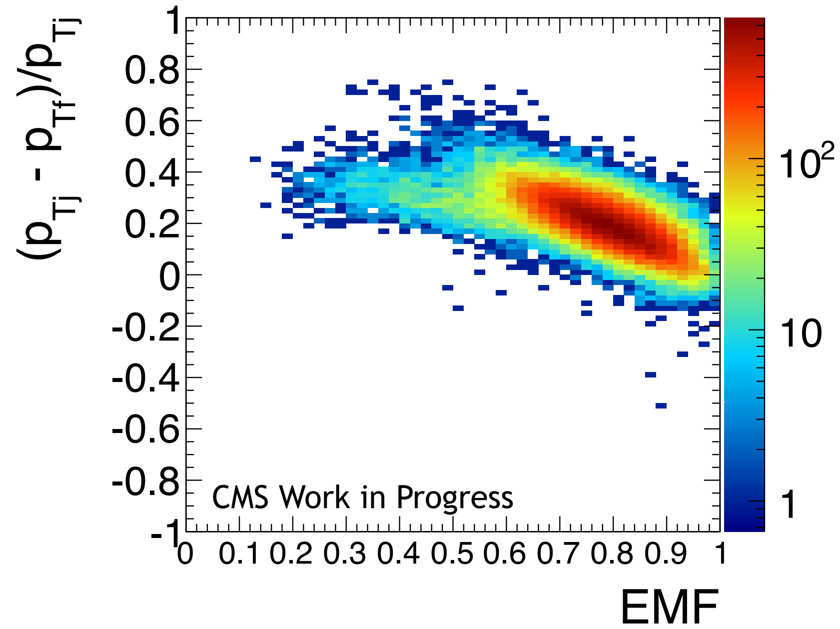

Leading γ

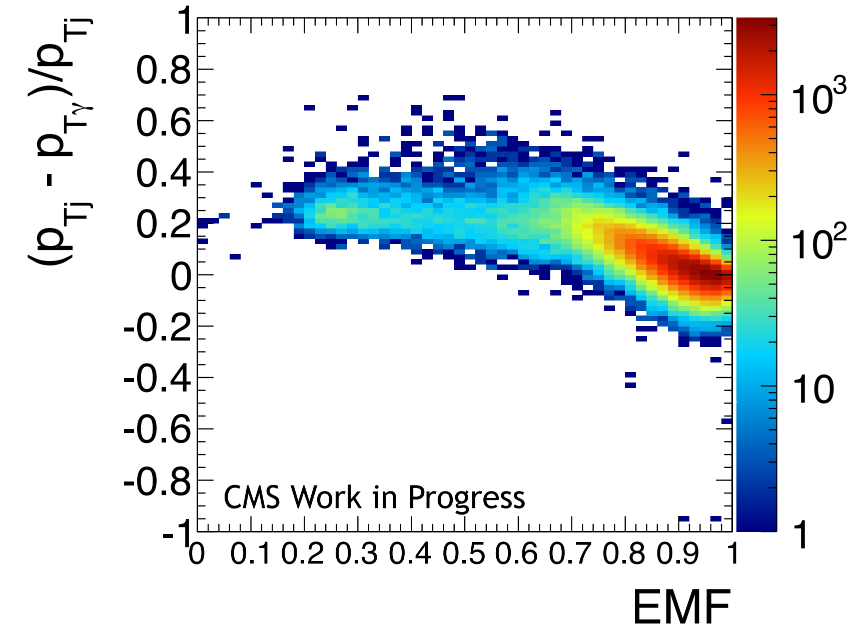

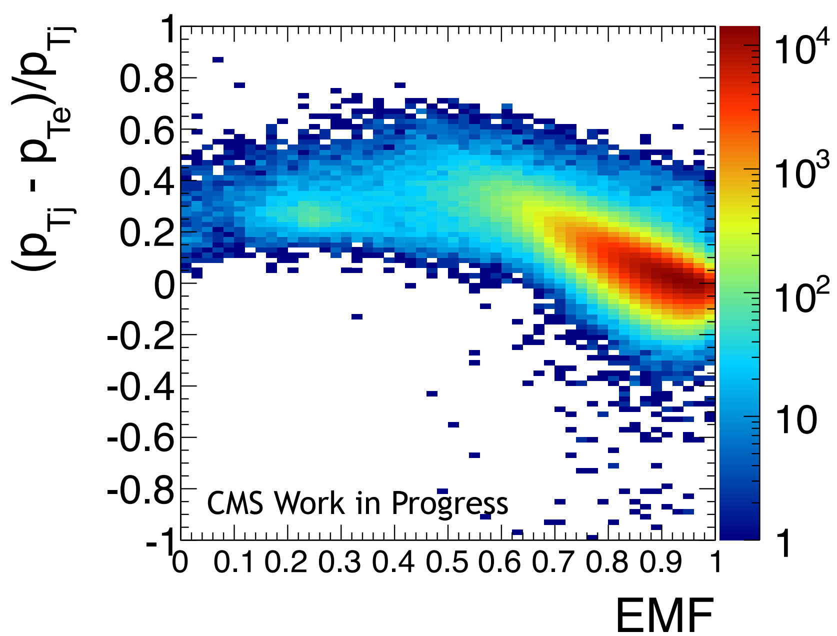

Trailing e

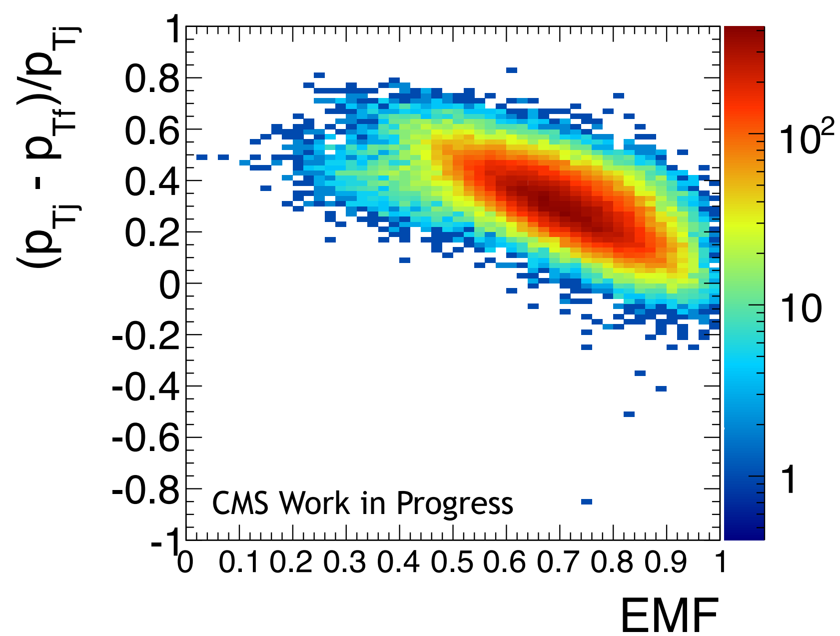

Trailing f

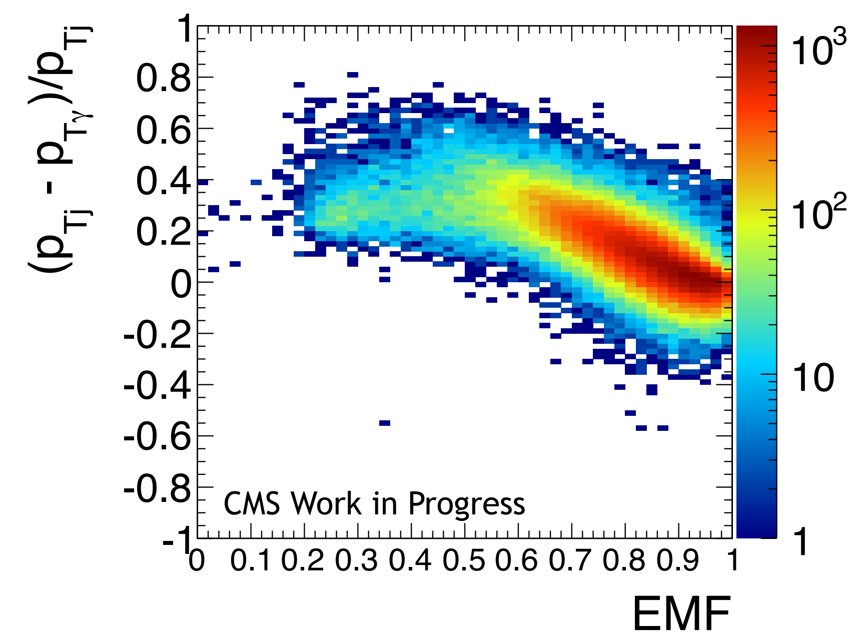

Trailing γ

PF vs. ECAL E_T (2)

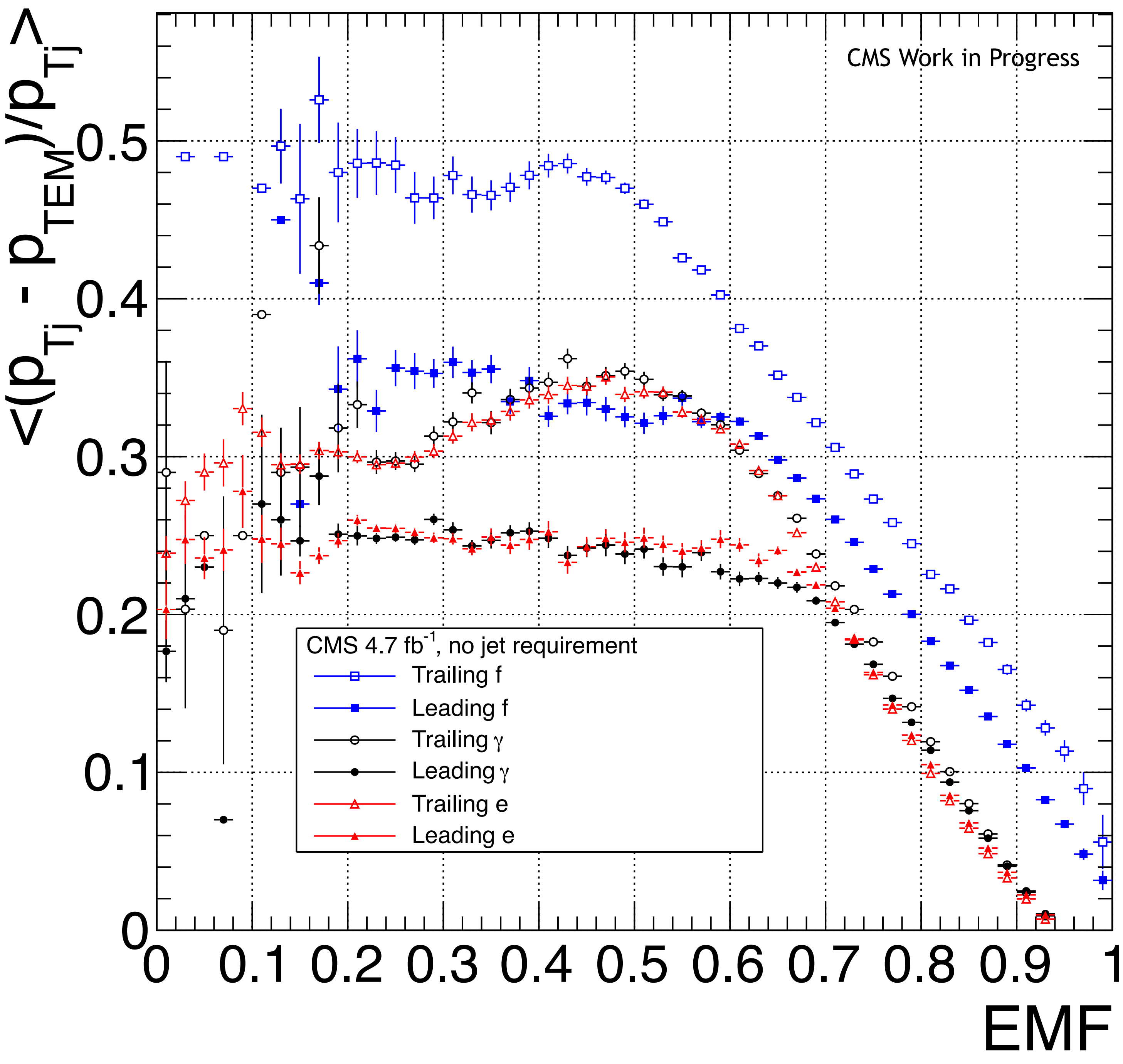

- Profile histograms of previous slide

Di-EM p_T weights

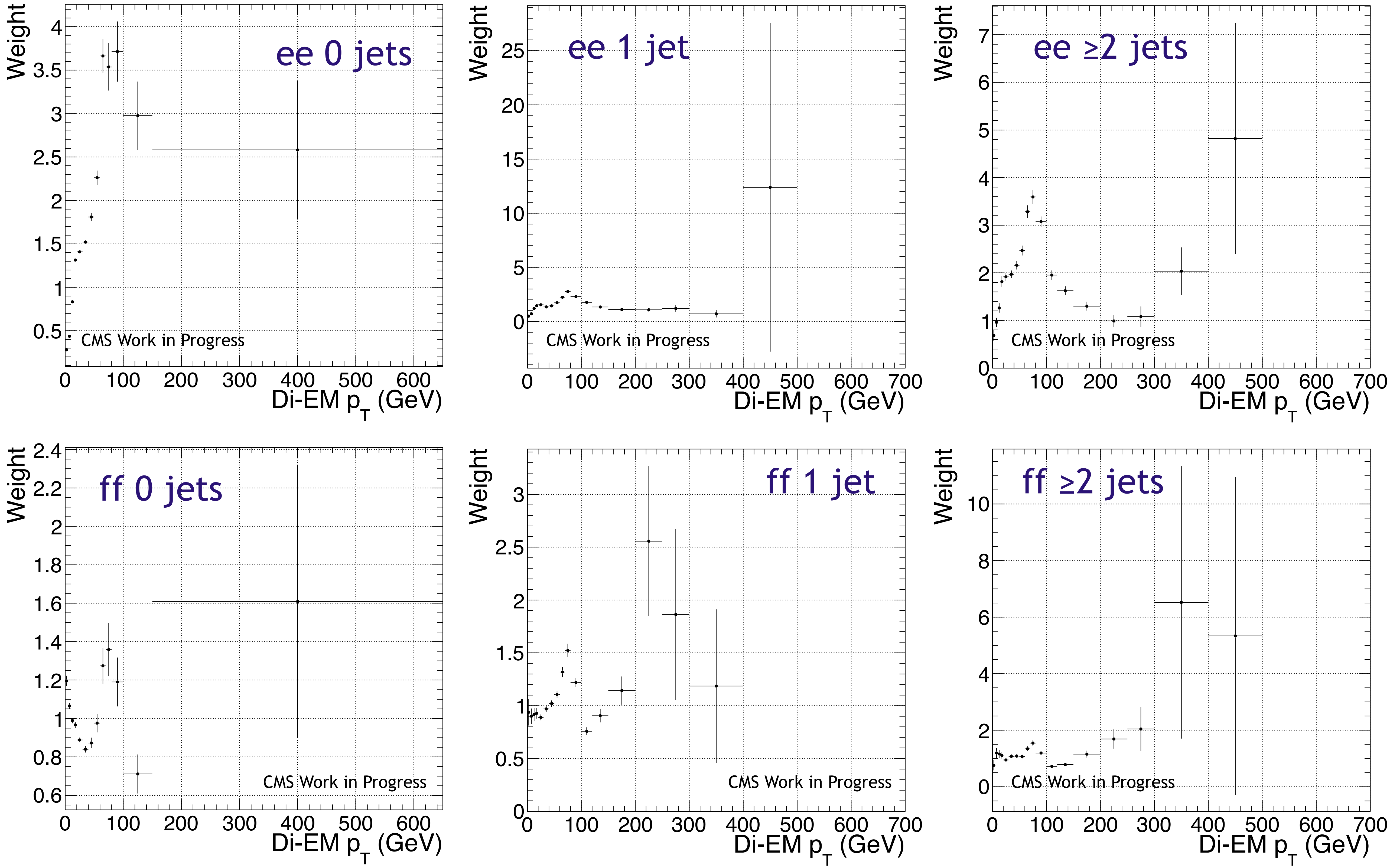

Removing ttbar from the ee sample

- ee sample contains a non-negligible high-ME_T background of ttbar events
- 71 GeV ≤ m_{ee} < 81 GeV and 101 GeV ≤ m_{ee} < 111 GeV sidebands used to estimate the non-Z background in the 81 GeV ≤ m_{ee} < 101 GeV ee sample
  - Reweight the low and high sidebands independently, using weights derived from events in those sidebands
  - Subtract the low and high sideband ME_T distributions from the Z signal ME_T distribution
  - Proceed with normalization of the sideband-subtracted ee sample

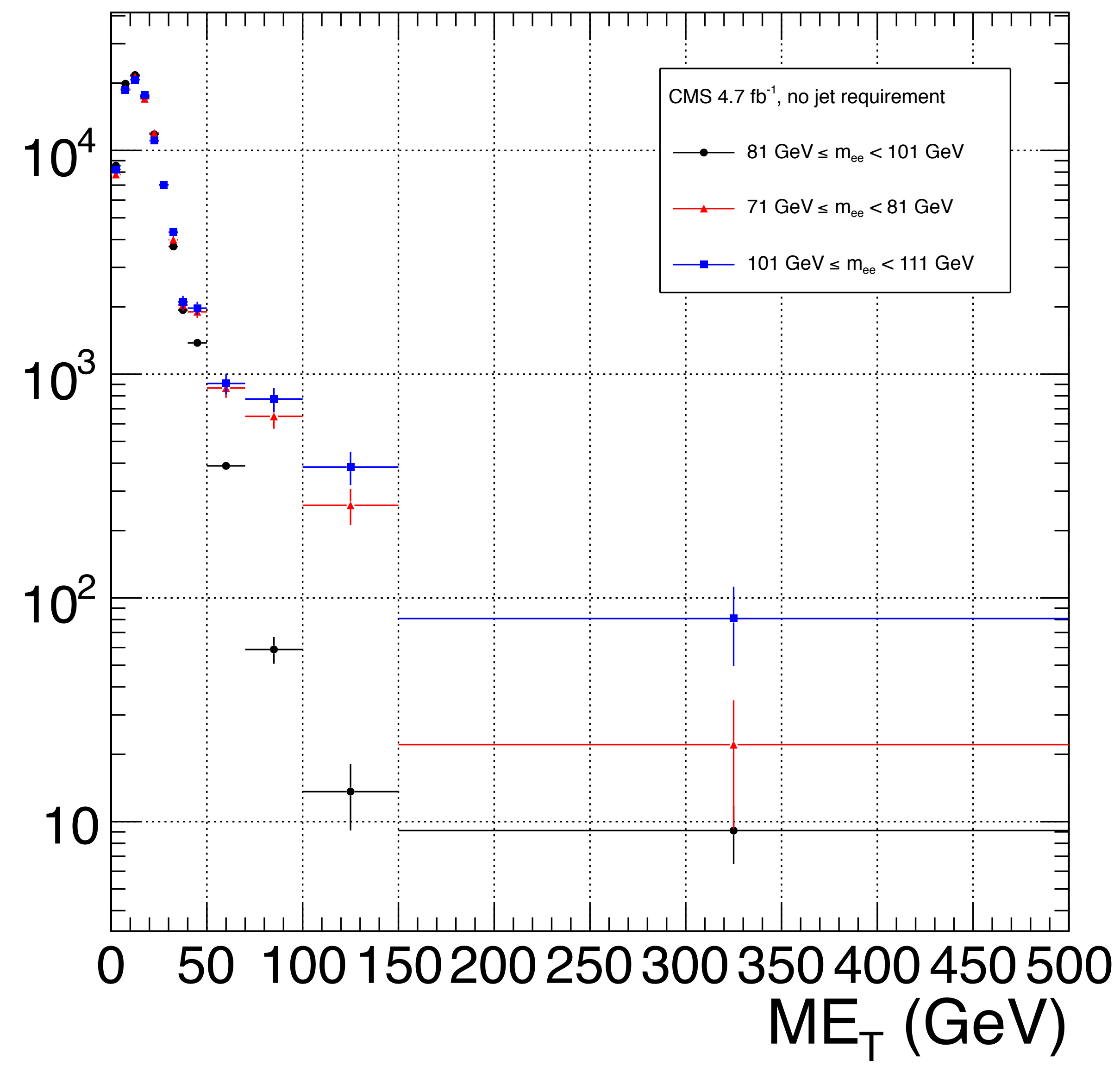

ee sideband weights

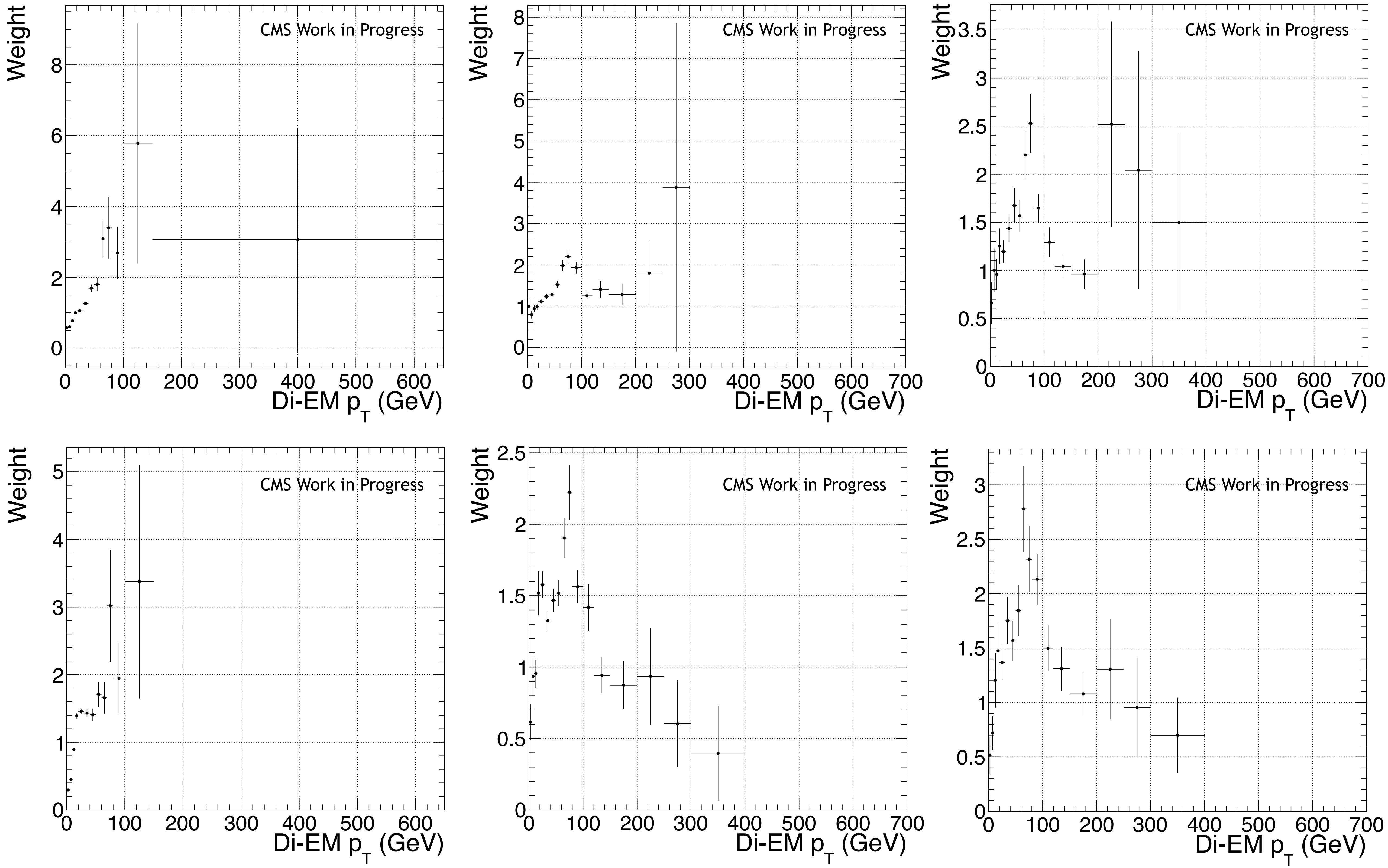

$f_{e \to \gamma}$ calculation

The number of events in the di-electron sample is given by

$$N_{ee} = f^2_{e \to e} N_{Z \to ee}$$

where $f_{e \to e}$ is the efficiency to correctly identify an electron via pixel match and $N_{Z \to ee}$ is the true number of Z→ee events. The number of events in the eγ sample due to misidentification of 1 Z electron as a photon is given by

$$N^Z_{e\gamma} = 2 f_{e \to e}(1 - f_{e \to e}) N_{Z \to ee}$$

Solving for $f_{e \to e}$,

$$f_{e \to e} = \frac{1}{1 + \frac{1}{2}\frac{N^Z_{e\gamma}}{N_{ee}}}$$

The number of events in the eγ sample due to correctly identifying a W electron is given by

$$N^W_{e\gamma} = f_{e \to e} N_W$$

where N_W is the number of true W→eν events. The number of $\gamma\gamma$ events from W electron misidentification is given by

$$N^{EW}_{\gamma\gamma} = (1 - f_{e \to e}) N_W$$

where we have neglected the contribution from Z electron misidentification since it is small (i.e., $f_{e \to \gamma}$ is small and the Z contribution involves $f^2_{e \to \gamma}$, since both electrons have to be misidentified). Since

$$f_{e \to e} = 1 - f_{e \to \gamma}$$

solving for $N^{EW}_{\gamma\gamma}$

$$N^{EW}_{\gamma\gamma} = \frac{f_{e \to \gamma}}{1 - f_{e \to \gamma}} N_{e \to \gamma}$$

GMSB MC

- Signal spectrum generation via SuSpect v2.41 [23]
- Signal decays via SDECAY v1.3 [24]
- Event generation, parton showering, hadronization, and decay via Pythia 6 [25]
- CMS detector simulation (GEANT [26]) and reconstruction
- Gravitino LSP
- NLO production cross sections and renormalization and factorization scale uncertainties calculated with Prospino
- PDF uncertainties calculated using PDF4LHC [27] recommendations
- 2 different signal scenarios
  - Bino NLSP (1): M_1 = 375 GeV, M_2 = 3.5 TeV, tan β = 2, squark and gluino masses in [400 GeV, 2000 GeV], sleptons and all gauginos except the lightest neutralino have mass 3.5 TeV, heavy right-handed squarks (GGM sum rules)
  - Bino NLSP (2): M_1 = 375 GeV, light squarks ~2.5 TeV, M_3 in [300 GeV, 2000 GeV], M_2 in [200 GeV, 1500 GeV]

References

1. http://cdsweb.cern.ch/record/929101/files/oreach-2001-001_01.jpg
2. *CMS: The Electromagnetic Calorimeter Technical Design Report*, ed. F. Pauss, CERN/LHCC 97-33 (1997).
3. CMS Collaboration, *CMS ECAL Performance on 2011 Data*, CERN-CMS-DP-2012-002 (2012).
4. http://cdsweb.cern.ch/record/936376/files/oreach-2004-002_04.jpg
5. http://cdsweb.cern.ch/record/1299085/files/VPT_RIE_front.jpg
6. K.W. Bell et al., *Vacuum Phototriodes for the CMS Electromagnetic Calorimeter Endcap*, IEEE Trans. Nucl. Sci. **51** (2004) 5.
7. Courtesy D. Phillips.
8. M. Akrawy et al., *Development Studies for the OPAL End Cap Electromagnetic Calorimeter Using Vacuum Photo Triode Instrumented Leadglass*, NIM **A290** (1990) 76.
9. G. A. Akopdzhanov, A. V. Inyakin, and P. S. Shuvalov, *Photomultiplier Short-Term Instability*, NIM **161** (1979) 247.
10. CMS Collaboration, *ECAL 2010 Performance Results*, CERN-CMS-DP-2011-008 (2011).
11. CMS Collaboration, *The CMS Experiment at the CERN LHC*, JINST **3** (2008) S08004.
12. Courtesy A. Ledovskoy.

References

13. S. P. Martin, *A Supersymmetry Primer*, arXiv:hep-ph/9709356 (1997).
14. http://pdg.web.cern.ch/pdg/cpep/images/sypersymmetry.gif
15. M. Cacciari, *FastJet: a code for fast k_t clustering, and more*, LPTHE-P06-04 (2006).
16. Yu. Blinnikov et al., *Radiation hardness, excess noise factor and short-term gain instability of vacuum phototriodes for the operation in pseudorapidity range 1.5 < η < 3.0 at CMS ECAL*, NIM **A504** (2003) 228.
17. A. García-Bellido, *Searches for gauge mediated SUSY breaking at LEP*, in Proceedings of the 10th International Conference on Supersymmetry and Unification of Fundamental Interactions, Hamburg, 2002 (unpublished).
18. B.C. Allanach et al., *The Snowmass Points and Slopes: benchmarks for SUSY searches*, Eur. Phys. J. **C25** (2002) 113.
19. V. Abazov et al., *Search for Diphoton Events with Large Missing Transverse Energy in 6.3* fb^{-1} *of ppbar Collisions at* $\sqrt{s} = 1.96$ *TeV*, Phys. Rev. Lett. **105** (2010) 221802.
20. B. Brau, *Tevatron Searches for New Physics with Photons and Jets*, arXiv:1007.2244v2 [hep-ex] (2011).
21. CMS Collaboration, *Measurement of the Isolated Prompt Photon Production Cross Section in pp Collisions at sqrt(s) = 7 TeV*, CERN-PH-EP/2010-053 (2010).

References

22. CMS Collaboration, *Photon Reconstruction and Identification at √s = 7 TeV*, CMS-PAS-EGM-10-005 (2010).
23. A. Djouadi, J.-L. Kneur, and G. Moultaka, *SuSpect: A Fortran code for the supersymmetric and Higgs particle spectrum in the MSSM*, Comput. Phys. Commun. **176** (2007) 426–455.
24. M. Muhlleitner, *SDECAY: A Fortran code for SUSY particle decays in the MSSM*, Acta Phys. Polon. **B35** (2004) 2753–2766.
25. T. Sjöstrand, S. Mrenna, and P. Z. Skands, *Pythia 6.4 Physics and Manual*, JHEP **0605** (2006) 026.
26. J. Allison et al., *Geant4 developments and applications*, IEEE Trans. Nucl. Sci. **53**, 270 (2006).
27. M. Botje et al., *The PDF4LHC Working Group Interim Recommendations*, arXiv:1101.0538v1 [hep-ph] (2011).